ULTRAFAST LASER WRITTEN BULK WAVEGUIDES AND GRATINGS

by

Sandy Ng

A thesis submitted in conformity with the requirements
for the degree of Master of Applied Science
Graduate Department of Electrical and Computer Engineering
University of Toronto

Department of Electrical and Computer Engineering
University of Toronto, Sandy Ng, MASc 2000

ULTRAFAST LASER WRITTEN BULK WAVEGUIDES AND GRATINGS

ABSTRACT

The field of photonics has been growing tremendously in popularity and market share within the past few years. It has moved beyond the telecommunications market to encompass many different applications, yet industry generally views photonics as still lagging behind microelectronics by ten to twenty years. To follow in the footsteps of electronics, photonics must become miniaturized and integrated. The nonlinear absorption of ultrafast lasers confines laser-matter interaction in three dimensions, permitting the exploration of three-dimensional integrated optics.

This thesis studies the effects of scan speed, repetition rate, fluence, accumulated fluence, and sample material on laser-induced refractive-index modulations. The results extend current research by covering a larger parameter range and are compared with deep-ultraviolet F_2 results to evaluate the efficiencies of these two forefront processes. This thesis also characterizes bulk waveguides in terms of transmission and scattering loss measurements. These results suggest processing parameters for commercialization of the waveguides.

General conclusions of this thesis are that a higher repetition rate and tighter focus have the potential to induce higher index changes, although they also increase the likelihood of causing damage. The processing window for fused silica is quite small: the upper limit is a fluence of ~13 J/cm^2, and number of pulses $<10^5$. The lower limits have not yet been identified.

ACKNOWLEDGEMENTS

Once upon a time ... there was a graduate student named Sandy Ng. This is her message:

> I wish to thank those at the University of Toronto who helped me in my thesis work. These include my supervisor, Professor Peter Herman, who provided guidance and direction; and my fellow lab members: Igor Konovalov, Sola Ness, Christian Lauer, Jie Zhang, Kevin Chen, Santiago Camacho, Jeff Czapla-Myers, Detleff, and Dirk Schaeffer who were my peers and friends during my time here. I would particularly like to recognize Dragan Coric and Markus Lapczyna for their support and inspiration.
>
> I would also like to acknowledge Dr. Paul Corkum at NRC, who generously allowed me access to his femtosecond laser, and Dr. Manjusha Mehendale, who operated the laser and assisted with and conducted the experiments.
>
> To all my family and friends in Vancouver and Toronto: thank you for sharing your patience and knowledge. Salima has shared all my experiences of the last two years here, and Eddie has been my daffodil. Mommy, Daddy, and Baby ... !

After two long years, Sandy graduated ... and lived happily ever after. The end.

TABLE OF CONTENTS

LIST OF FIGURES

Number *Page*

LIST OF TABLES

Chapter 1

1 INTRODUCTION

The field of photonics has been growing tremendously in popularity and market share within the past few years [1]. It has moved beyond the telecommunications market to encompass many different applications including manufacturing, medicine, sensing, metrology, and biotechnology. The demand for photonics to replace electronics in telecommunications was initially fueled largely by the need for greater speed and capacity. However, photonics offers other advantages over electronics; advantages such as lower power consumption, less noise, and lower losses. Yet industry generally views photonics as still lagging behind microelectronics by ten to twenty years. To follow in the footsteps of electronics and grow to support a wide variety of industries, photonics must become miniaturized and integrated.

1.1 Integrated Optics

In 1969, the AlGaAs semiconductor laser was realized. It was the first laser source small and cost-effective enough for mass production. In 1970, low-loss optical fiber provided the medium over which the laser light could be transmitted for useful distances [2]. These two advances in photonics provided the necessary technologies for the development of fiber optic telecommunications.

Since that time, photonics has progressed from serving as the high-capacity backbone that delivers voice and data around the globe, to an integral part of numerous new technological

devices in the 1990's. The manufacturing precision offered by photonics is essential to shape micron-sized channels and waveguides for the test and measurement of chemical reactions in lab-on-a-chip applications [3]. The transmission bandwidth and the resilience from electromagnetic interference of photonics is now required in the optical interconnects inside high-speed computers. The enormous transmission capacity of photonic components is facilitating the explosion of data transfer through the Internet. The need for photonics in these and many other applications, coupled with the decreasing cost of production, has placed photonics in a position to supplant electronics in many leading high technology domains.

However, this succession of electronics has not and will not occur overnight. The electronics industry is well established, with efficient production methods, extensive manufacturing facilities, and a support structure ranging from design software to an educated task force. This has not always been the case; the semiconductor industry developed from large vacuum tubes and copper wires. Photonics is now in the central stages of a similar "microelectronics-type" development. What were once discrete optical components connected through plastic jacketed fibers, are now miniaturized components within those fibers (e.g. fiber Bragg gratings, fiber lasers).

The next step is the development of planar and three-dimensional integrated optics. Integration leads to miniaturization, which is important in industry to packaging into various personal devices and in large quantities into telecommunications racks. Integration also reduces manufacturing costs by eliminating assembly of discrete components. Conversely, discrete components can be incorporated onto integrated optical boards.

Silica is one material of choice for planar integrated optics because it is economical, has low loss, and is available in smooth, flat, large pieces. It is compatible with the optical fiber refractive index and thermal expansion coefficient. It is stable and its refractive index is

controllable. It is also compatible with silicon fabrication techniques in processing microelectronic chips. Additionally, the silicon optical bench (SiOB) (silica on silicon) onto which optoelectronics, such as lasers, can be mounted is a quickly growing industry.

1.2 Schools of Practice

Currently, integrated photonic devices in glasses are produced through plasma etching or ion exchange to define waveguides in one or several planes in glass.

A different method of producing integrated optics is through the use of laser-induced index modification. Beyond being already a successful method for the rapid prototyping of photonic components, this method has the potential to free integrated optics from their planar form and move fully into three dimensions.

1.2.1 The Old Schools: Deposition and Patterning

The established production methods of integrating optics in silica involve depositing layers of glasses and patterning some of these layers through photolithography and etching. In large-scale production, deposition can be accomplished by:

- Chemical Vapour Deposition (CVD): CVD involves depositing a high-pressure vapour onto a surface through thermal activation. When this process is assisted by plasma, it is termed plasma enhanced chemical vapour deposition (PECVD). [4, 5]
- Flame Hydrolysis Deposition (FHD): In FHD, glass is deposited by hydrolysis of silicon chloride in a hydrogen flame. The process occurs at lower temperatures and faster deposition rates than CVD. [4, 5]
- Sol-gel: A silica sol is gelled and then dried and sintered. The advantage of sol-gel is the intermixing of particles on an atomic scale, which allows a larger range of dopants

to be incorporated into glasses. This process is performed at low temperatures compatible with the integration of electronic components. [6, 7]

Integrated optical circuits can be imprinted onto glasses through a photoresist mask by etching or ion-exchange:

- Reactive Ion Etching (RIE): A pattern is imprinted into the photoresist through photolithography, and a plasma etch is applied to remove the glass not protected by the photoresist. [4, 5]
- Ion-exchange: Patterning by ion-exchange is more complicated than etching. Plasma and chemical etches are applied to remove various layers in the pattern of the photoresist. The sample is subjected to high-temperatures, and sometimes an electric field, in the presence of a salt melt (Ag+, K+, Cs+, Tl+). Ions diffuse into the exposed glass and replace Na+ ions. [8]

1.2.2 The New School: Laser-writing

Three-dimensional (3D) integrated photonics began as an extension of two-dimensional (2D) photonics onto several planes; layers were patterned one on top of another. The above methods of production are multi-step processes and still somewhat "2.5D" limited, i.e. not completely free in the third dimension. 3D photonic devices have grown to include interaction between layers, but fabrication remains highly layered in nature [5].

Complex procedures and expensive equipment are involved in current 2D production methods. Further, the existing procedures do not provide for the trimming of specific components, an important need for wavelength-sensitive photonic devices. A direct-write method is therefore valuable for future manufacturing and prototyping because of its greater

flexibility. Figure 1-1 illustrates the simplicity of a direct laser-write in comparison with current multistep approaches.

Traditionally, UV lasers have been used to induce index changes in glasses because glasses are more photosensitive to shorter wavelengths. Higher index changes (<0.0004) have been achieved with the 157-nm excimer laser than with any other UV laser (193 or 248 nm) [9-11]. Studies have been conducted in this lab by Zhang into the use of the 157-nm fluorine (F_2) laser for writing planar circuits and volume gratings [12]. Chen in this same lab has induced much higher index changes (< 0.005) under the same accumulated fluences in germanosilicate glass [12]. However, the linear absorption responses of these processes restrict the laser-glass interaction to either the near surface region or doped regions of higher absorption such as buried germanosilicate waveguides.

On the other wavelength extreme, the 800-nm ultrafast laser induces a multi-photon response that allows laser-glass interactions to be focussed into the bulk of a material.

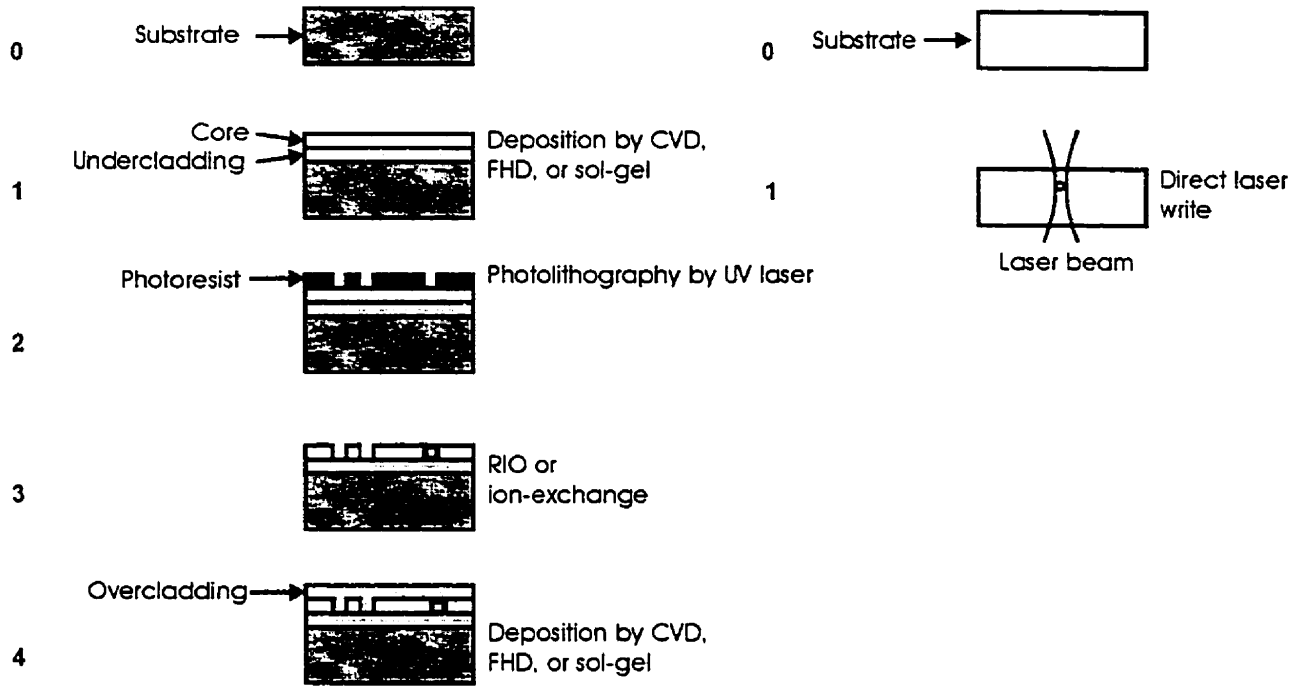

Figure 1-1 Comparison of fabrication steps of buried waveguides by conventional (left) and ultrafast laser (right) methods illustrating the simplicity of a direct-write method.

1.3 The Ultrafast Solution: 3-D optics becoming reality

An ultrafast laser deposits energy nonlinearly into glasses, which permits the modification of refractive index in a highly localized volume within the bulk. The use of ultrafast lasers to write index changes is currently being explored for applications in bit-patterned memory, waveguides, and other photonic devices in both bulk glasses and fibers [13, 14].

The use of ultrafast lasers to write index changes was first described by Hirao and coworkers [15] with waveguides and Mazur and co-workers [16] with memory bits. For three years, these two groups attempted to determine the mechanism of index modulation by ultrafast laser. In 1999, other research groups began to expand the field by exploring laser processing variables: Sung Hak et al. [17] have exploited self-channeling to write a double cladding within a multimode fiber, Homoelle et al. [18] have studied the effects of processing parameters on the index changes with waveguides and have written a Y-coupler, Sudrie et al. [19] have fabricated birefringent structures by controlling laser polarization, and Sikorski et al.

[14] have demonstrated amplification by writing in doped glass, and Kondo et al. [20] have recently written long-period gratings inside fiber.

Photonic devices have moved from a miniaturization of geometric optics to more integrated, compact structures such as fiber Bragg gratings (FBGs). However, these devices are not scalable; for example, doubling the number of channels of an FBG demultiplexer requires doubling the number of FBGs and attaching them in series. With the development of arrayed waveguide gratings (AWGs), demultiplexers have moved towards a 2D solution.

Confinement of ultrafast laser interaction in three dimensions gives full three degrees of freedom and so permits the exploration of three-dimensional integrated optics. One goal of this lab is the development of diffractive three-dimensional (3D) free-space devices. By processing input in one stage, they offer the advantage of parallel processing, which permits higher throughput. So, laser-written diffractive 3D free-space devices offer parallelism to allow scalability.

1.4 Overview

This thesis aims to contribute in two projects: one is the development of diffractive 3D photonic devices, and the other is the development of processing tools for ultrafast-writing of waveguides.

The writing of 3D devices requires precise control over refractive index modulations. To that end, this thesis studies the effects of scan speed, repetition rate, fluence, accumulated fluence, and sample material on laser-induced refractive-index modulations. The index change is calculated from the measurements of numerical aperture in bulk waveguides and diffraction efficiency in planar gratings. The results extend current research by covering a

larger parameter range and are compared with deep-ultraviolet F_2-laser results to evaluate the efficiencies of these two forefront processes.

The fabrication of waveguides for industry requires optimization of system variables. This thesis characterizes bulk waveguides in terms of transmission and scattering loss measurements. These results provide recommended processing parameters for commercialization of the waveguides.

Chapter 2 introduces the past and current research into ultrafast laser absorption and photosensitivity mechanisms in glasses. Recent applications of ultrafast-induced index modifications are also introduced. The experimental arrangement for writing and characterizing the bulk waveguides and gratings are described in chapter 3. This includes a waveguide coupling system, designed and built specifically for this thesis. Chapter 4 details the results from characterization, and chapter 5 discusses the implications of these results on processing parameters. In particular, an explanation of the effects of repetition rate on index change is hypothesized and new processing windows are suggested. Conclusions in chapter 6 point future work towards better characterization techniques and new processing parameters.

Chapter 2

2 REFRACTIVE INDEX CHANGES - BACKGROUND

2.1 Introduction

The phenomenon of refractive index changes due to laser illumination was first discovered by Hill and coworkers [21] at Communications Research Canada (CRC) in Ottawa in 1978. Since that time, the photosensitivity of glasses to ultraviolet (UV) radiation has been exploited for the production of fiber Bragg gratings for use in filters, fiber sensors, fiber lasers, and many other photonic devices [22]. More recently, with the commercialization of higher power ultrafast lasers, many research groups have begun experimenting with the use of these infrared (IR) lasers to write index change [13, 14, 19, 20, 23, 24]. Femtosecond pulses have been able to induce higher index changes and confine them within the bulk of transparent materials.

The first groups using ultrafast lasers to induce index changes in glasses wrote simple structures: waveguides [15] and bit-patterned memory [25]. Their research focused on the underlying physics of the reaction, from which two streams of thought have developed: to extend the theories of UV photosensitivity to ultrafast photosensitivity, such as compaction and the formation of defects; and to extend the theories of ultrafast processing to a gentler, lower-energy regime. Now, research has shifted towards gaining control of this process and finding new applications. To this end, more complex devices have been written and characterized, such as mode couplers and fiber Bragg gratings [14, 17-20].

2.2 Absorption Mechanism in Glasses

Absorption by most glasses of ultrafast infrared (IR) light at ~800 nm cannot be explained by conventional single photon absorption processes, as is the case for UV light. However, the absorption of IR photons, as well as the volume localization of ultrafast interaction with glasses, can be explained by nonlinear absorption.

UV absorption can be single photon and therefore linear. The absorbed power of light is directly proportional to the intensity of the laser integrated over the cross-sectional area of the beam. This is simply the power of the beam, which is constant over propagation distance, so the absorption of the beam is constant throughout the beam path as is illustrated in Figure 2-1 b. Provided the integrated intensity is above a threshold, there will be index modulation.

In a nonlinear process, absorption is dependent on a power of the laser beam intensity and is largest at the beam waist where the intensity is highest. Only that portion of the beam at which the integrated intensity is above a threshold interacts with the glass as shown in Figure 2-1 c. This confines the index modulation to a volume centered around the beam focal volume.

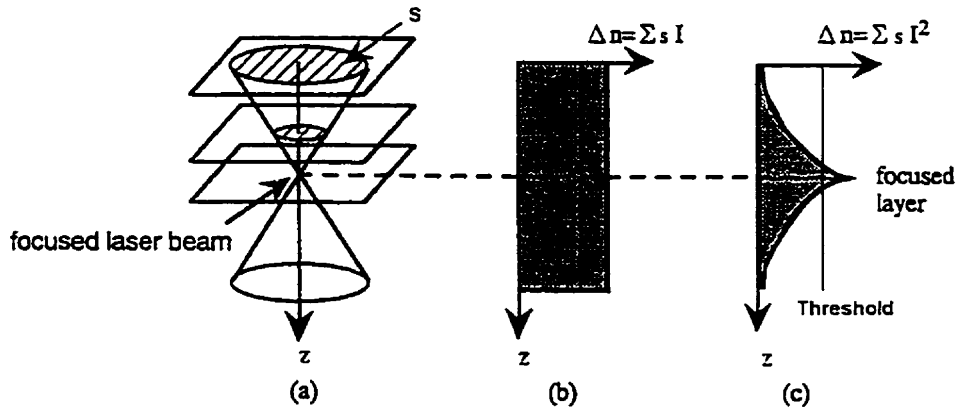

Figure 2-1 Localization effect of multiphoton absorption through dependence on a power of the intensity (modified from [26]). The geometry of a laser beam is shown in (a). The magnitude of absorption along the laser axis in (b) linear processes is constant and (c) nonlinear processes is highest at the focal point.

Nonlinear processes require high intensities because the probability of their occurrence is dependent on photon flux. More than $5x10^{12}$ W/cm^2 is necessary for formation of plasma in microexplosions, an event coined by Mazur and coworkers to describe the localized formation of plasma and permanent index change when writing bit-patterned memory. Ultrafast lasers (< ~200 fs) reach the necessarily high intensities to initiate multiphoton absorption by their short pulse width, especially when focused. Proposals for nonlinear glass absorption mechanisms of ultrafast pulses include: tunnel ionization, multiphoton ionization, and electron avalanche.

2.2.1 Tunnel ionization

At short laser pulse widths (<~40 fs), a possible means of laser absorption is tunnel ionization (TI) [27, 28]. The electric field supplied by the laser is below that necessary to ionize the electron. The adiabaticity or Keldysh parameter (γ) divides the TI and multiphoton ionization regimes:

$$\gamma = \sqrt{\frac{I_o}{2 \cdot U_p}} = \frac{\varpi_{laser}}{\varpi_{tunnel}} << 1 \qquad (2\text{-}1)$$

It is related to the ratio of the ponderomotive or oscillation energy of the electron in the field of the laser (U_p) to the ionization energy of the electron (I_o). It must be much smaller than unity for TI to occur.

The latter half of the equation states that another condition for TI is that the tunneling time is much less than the optical period. In essence, TI takes place when the electric field of the laser can be considered constant over the tunneling time. While this "static" field is insufficient to cause the electron to flow over the potential well, the electric field distorts the electron potential so that on one side the well becomes a barrier through which the electron can tunnel and escape. The solid arrowed lines represent the tunneling electrons.

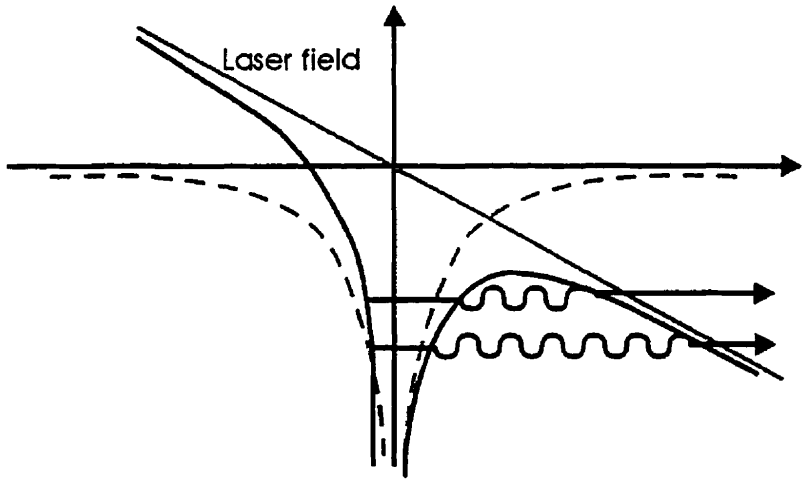

Figure 2-2 Effect of laser electric field (solid grey line) in distorting electron potential (dotted grey lines) and facilitating TI (after [28]). At the two energy levels shown, the field has been distorted enough to permit electrons to tunnel through the barrier (solid black lines).

2.2.2 Multiphoton ionization

Multiphoton ionization (MPI) is the simultaneous absorption of more than one photon from a beam such that a bound electron is ionized. This phenomenon is under research for use in photorefractive materials to write bit-patterned memory, such as in recordable compact

disks [29, 30], and in photoreactive chemicals to induce internal reactions, such as the release of a drug within the body [31].

Each ultrafast IR photon, with its long wavelength and low photon energy (~1.6 eV), has insufficient energy to excite an electron across the bandgap of fused silica (~ 10 eV). However, MPI is a process in which the summary absorption of several photons excites electrons from the valence into the conduction band. Figure 2-3 compares nonlinear absorption with linear absorption graphically.

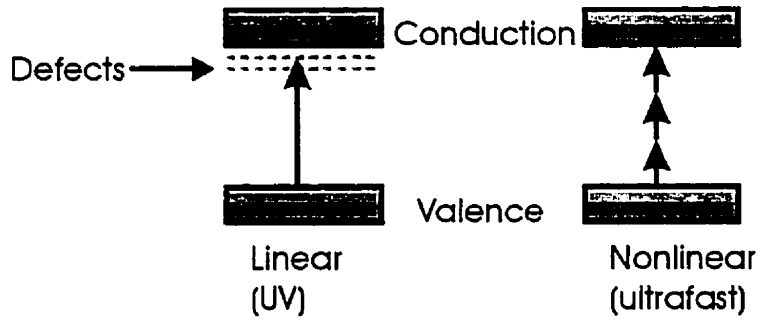

Figure 2-3 Single photon (left) versus multiphoton (right) absorption in glasses. A UV photon has sufficient energy to excite electrons across the bandgap, but an IR ultrafast photon does not. Multiple IR photons can be absorbed to sum to sufficient energy.

2.2.3 Electron avalanche

Electron avalanche is initiated by an absorption mechanism such as TI or MPI. Once an electron is excited into the valence band by one of these processes, it can linearly absorb additional energy and collide with other electrons causing impact ionization. More electrons are excited across the bandgap, which in turn cause additional ionization, resulting in the eventual formation of a plasma. At shorter pulse widths, there is insufficient time for collisions to occur. In such cases, it is possible that TI or MPI alone can form the plasma [32].

2.3 Photosensitivity Mechanism in Glasses

Photosensitivity is defined as the susceptibility of a material to refractive index changes by exposure to light. The means of index change depends on the type of material. For example, $LiNbO_3$ is a photorefractive material. These materials have electron traps due to intrinsic defects or residual impurities. Electrons from these traps are excited by incident light into the conduction band, resulting in local index modification.

Many models for photosensitivity in glasses have been proposed [33]. The mechanism, however, remains to be explained satisfactorily. Two of the proposed theories, the formation of defects and compaction, were originally developed for UV and have now been applied to ultrafast laser-induced modifications.

2.3.1 Defect Formation

A popular theory for UV-induced index modulation in glasses is the formation of defects, namely, Si*E'* and Ge*E'* colour centres, non-bridging oxygen hole centers (NBOHC), and peroxy-radicals (POR). Electron spin resonance (ESR) tests are applied to gain information about the bond structure of the ultrafast laser-modified glasses. Figure 2-4 plots ESR results of UV-modified pure fused silica (top), silica with hydroxide (OH) (middle), and Ge-doped silica (bottom) [34]. The plots have absorption peaks corresponding to NBOHC, POR, and Si*E'* and Ge*E'* colour centre defects. Tests have shown all three previously mentioned defect types in ultrafast laser-modified glasses as well. This suggests that defect formation, which allows UV-induced index modulations, also allows ultrafast laser-induced index modulations. The formation of such defects by ultrafast laser, however, requires multiphoton absorption.

There have been suggestions that defect formation contributes only a minor role to index modulation [15], and the general consensus is that ultrafast laser-induced index changes are much more complex than UV photosensitivity.

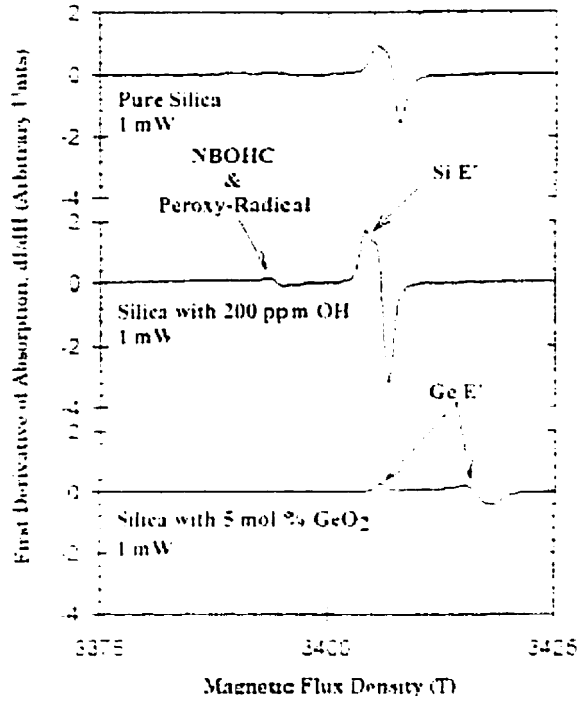

Figure 2-4 ESR results of silica glasses after irradiation with ultrafast laser (reproduced from Hirao [34]). Peaks corresponding to the presence of defects suggest defect formation as a means of index modification.

2.3.2 Compaction

Compaction has also been suggested as another mechanism of index change. Local heating of the glass is thought to melt a small volume, which resolidifies in a denser form, leaving the surrounding area less dense or strained. This idea is borrowed from the field of UV photosensitivity. Atomic force microscopy (AFM) has been used to map the cross sections of ultrafast laser-written waveguides [35]. Indentations in the centre of such structures indicate densification. The Raman spectra of ultrafast laser-written dots show a shift in the vibration mode of SiO_4, which is known to be related to densification [36]. Microellipsometry has been used to measure the index profile of waveguides [15]. A small

decrease in refractive index sometimes surrounds the central region of increased index supporting this model of compaction and expansion. Figure 2-5 plots the refractive index profiles of ultrafast laser-written waveguides scanned once (bottom) and ten (top) times. Both show lower indices adjacent to the central peak.

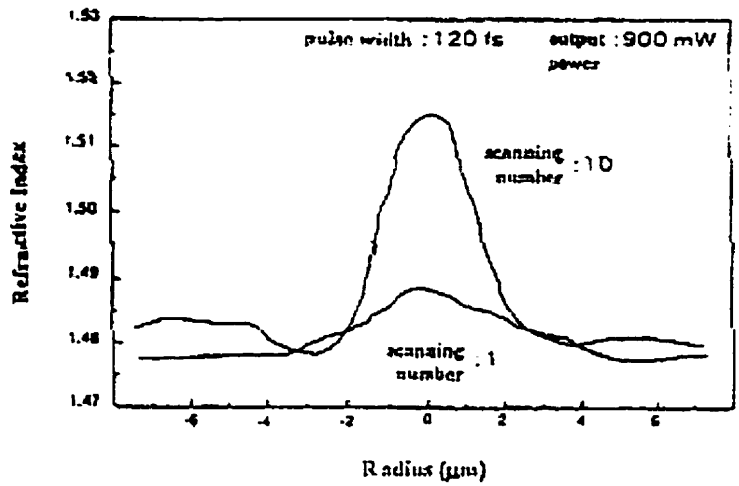

Figure 2-5 Refractive index profile of femtosecond-written waveguide (reproduced from [34]) showing central increase in index and surrounding decrease in index.

Mazur and coworkers have attempted a more detailed analysis of the mechanism for ultrafast laser-induced compaction and expansion. The group relates the ultrafast laser-matter interaction to explosion dynamics in water. The single pulse event consists of the following: absorption of photon energy, collision of excited electrons inducing electron avalanche ionization, formation of plasma, and rapid expansion of plasma causing a "microexplosion" and associated shockwave. A void is produced, surrounded by a higher density region. AFM and scanning electron microscopy (SEM) observations confirm this [16]. Such structures are in direct opposition to those mentioned in the previous chapter; however, Mazur's group has focussed to a smaller beam waist (~1 μm vs. ~10 μm) and their laser system is quite different as is described below. Often, phase changes

(amorphous to crystalline) are also observed. In fact, a broad range of phenomena occur under the heading of microexplosions[a].

The laser system used by the Mazur group to write gratings is, however, different from the system used in this thesis and by the majority of researchers in this field. While the pulse width is similar (100 fs), Mazur's group uses an unamplified laser at much lower energies (~nJ vs. ~μJ) and much higher repetition rates (~MHz vs. ~kHz) than others'. At such high repetition rates, the diffusion distance (d_{diff}) of the heat affected zone is submicron:

$$d_{diff} = \sqrt{4 \cdot D \cdot t} \tag{2-2}$$

where D is the diffusion rate (~0.9 μm/s for fused silica) and t is the time between pulses (40 ns for 25 MHz repetition rate). During the writing of index modulations, the small pulse energies allow a gentle deposition of energy to melt the focal volume, which resolidifies in denser form.

The thermal effect may be similar to that observed in laser micromachining where high repetition rates or *burst machining* produce a heated region for the laser to interact with [12].

2.4 Ultrafast Photosensitivity Applications

The Hirao Active Glass Project in Kyoto, Japan began publishing papers on ultrafast laser-written waveguides in 1996 [15]. It has a history of UV photosensitivity research and so applied many UV techniques, such as ESR, to their research. Mazur's group at Harvard, which has a history of ultrafast laser dynamics research, began publishing papers on ultrafast-laser written 3D memory also in 1996 [25]. Focusing on science rather than

[a] Microexplosions are not further discussed because they have not been directly applied to the writing of waveguide-type structures. For more information regarding microexplosions for the writing of 3D bit memory,

engineering, this group attempted to find the threshold energy of the plasma formation and correlate the shape of the index modulation with the dynamics of microexplosions. Within the past two years, several groups have reproduced and extended Hirao's and Mazur's results and shifted the field towards application to devices.

2.4.1 Waveguides

Waveguides are an important element of optical integrated circuits, forming the basis of many photonic components and connecting different of these devices together. The Hirao group has captured the near field profile of his waveguides, demonstrating both single and multimode transmission [34].

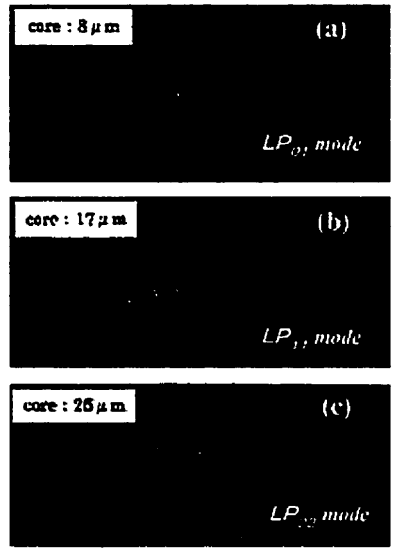

Figure 2-6 Mode profiles of variable diameter waveguides (reproduced from [34]) produced by ultrafast lasers. Single and multimode waveguides have been demonstrated by control of laser power.

The group has also determined the contributions of several parameters, for example, core diameter increases with increasing power, resulting in the single and multimode waveguides as shown in Figure 2-6. Other effects are listed in Table 2-1.

---

please refer to [37-41]

Table 2-1 Effect of various laser parameters on waveguide properties summarized from [42].

	EFFECT on WAVEGUIDE	
LASER SETTING	**Diameter**	**Index modulation**
Power	Directly proportional	Unknown
Number of passes (accumulated fluence)	None	Directly proportional
Pulse width (peak power)	None	Inversely proportional

The separation of laser variables into those that determine core diameter and those that determine index change provides the prospect of engineering waveguides of designed diameter and index modulation.

2.4.2 Other Applications

Within the past two years several research groups have begun to experiment with using ultrafast lasers to write photonics devices in glasses. Clark MXR is marketing their ultrafast laser to industry for writing features inside transparent materials. The following list gives a brief overview of these recent applications.

- Several groups [23, 25, 43] have used ultrafast lasers to imprint dots of index change in fused silica for 3D memory. Their results are quite similar: micron sized modulations with tens-of-microns layer spacing for easy readout. Currently achieved densities are on the order of 10^{10} bits/cm^3, which is comparable to that ofcompact disks (CDs have a single layer density of ~10^7 bits/cm^2) and digital versatile disks (DVDs have two layers ~40 μm apart with a single layer density of 10^8 bits/cm^2). The presently projected writing density limit of ultrafast laser-written memory is 10^{13} bits/cm^3 with several hundreds of nm diameter feature size. Commercialization still requires the standardization of a readout method, which currently varies from third harmonic generation to the use of a simple light microscope.

- Polarization sensitive components have been written in fused silica [19]. A linearly polarized helium-neon laser (HeNe) travelling through a grating written by a linearly polarized ultrafast laser does not produce a diffraction pattern when the two polarization axes are the same. A birefringent area was also demonstrated by writing overlapping gratings. This was used successfully as a beam splitter for a femtosecond laser.
- Extending the idea of a waveguide, a Y-coupler has been written in fused silica by branching off a second waveguide at a 0.5 ° angle from the first [18]. Light from an argon ion (Ar+) laser was coupled into the structure and split approximately equally between the two branches.
- A mode coupler has been written in multimode a fiber [17, 24, 44]. An ultrafast laser was focused into the core of the fiber and plasma channeling induced an index change 5 μm in diameter over a distance of 9 mm. The modified fiber produced an output intensity profile much higher and more confined than before the modification, demonstrating mode conversion from high-order multimode to low-order multimode.
- Long-period fiber gratings (LPFG) have been written in single-mode fibers [20]. Transmission spectra showed losses of 10-20 dB around telecommunications wavelengths (1300-1700 nm). However, insertion losses are high (4 dB) and loss peaks are irregular due to an imperfect writing scheme. The LPFG can be temperature tuned and the index modulations are stable to high temperatures of 500 °C.
- An optical waveguide amplifier was written in Nd-doped glass [14]. A waveguide was written with a femtosecond laser, and an Ar+ pump amplified a fiber laser source with ~1 dB/cm gain.

2.5 Theoretical Tools and Assumptions

This thesis determines the magnitude of laser-induced refractive index changes over a range of laser parameters by considering two structures: waveguides and gratings.

2.5.1 Waveguides

The waveguides written in this thesis are assumed and confirmed by profiles to be single-mode. The single-mode condition is:

$$V < 2.405 \tag{2-3}$$

where V is the normalized frequency:

$$V = \frac{2\pi \cdot a \cdot n_1 \cdot \sqrt{2 \cdot \Delta n}}{\lambda} \tag{2-4}$$

and a is the waveguide radius, n_1 is the core refractive index, Δn is the index difference between the core and cladding, and λ is the transmitted light wavelength.

With a probe laser wavelength (λ) of 633 nm, a substrate of fused silica (n_1=1.45), and a waveguide radius (a) assumed to be half of the beam waist diameter of 3 μm, the maximum allowable index change (Δn) is 6×10^{-3} for the waveguide to be single mode. This index change value is large in comparison with previous published results and the near field intensity profiles of light coupled out of the waveguides in this thesis appear Gaussian, so the waveguides are assumed to be single mode.

One method of measuring refractive index change from a waveguide is by calculation from numerical aperture (NA) measurements, as was employed by Gaeta and coworkers [18]. The formula relating NA to index change (Δn) for a step index profile is:

$$NA = \sqrt{2 \cdot n \cdot \Delta n} \tag{2-5}$$

The maximum exit angle of light from the waveguide, Θ_{NA}, determines the NA of the waveguide. This angle is related to the largest angle that still supports total internal reflection (TIR), Θ_{TIR}, by geometry and Snell's law of refraction. Θ_{TIR} is also calculated from Snell's law. These angles are shown in Figure 2-7.

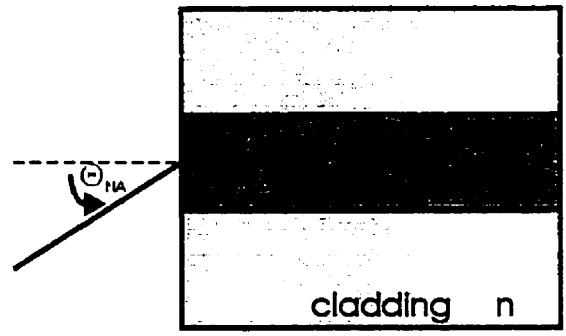

Figure 2-7 The relationship of the NA of a waveguide to the angle of TIR defines the relationship between waveguide core and cladding indices and the NA of the waveguide.

2.5.2 Gratings

Similarly to Mysyrowicz and coworkers [19], in this thesis the index modulation of gratings is calculated from diffraction efficiency measurements. The relationship between diffraction efficiency and index modulation is based on the Fresnel approximation of a far-field diffraction pattern of the electric field:

$$E(x,y,z) = \frac{j}{\lambda \cdot z} e^{-jk_o z} \int_{-\infty}^{\infty} dx' \int_{-\infty}^{\infty} dy' E(x',y',0) e^{-jk_o \frac{(x-x')^2+(y-y')^2}{2z}} \tag{2-6}$$

under the assumption:

$$\frac{[(x-x')^2+(y-y')^2]^2}{4 \cdot \lambda \cdot z^3} << 1 \tag{2-7}$$

where E is the electric field, λ is the probe wavelength, z is the direction of propagation, and the x and y axes form the plane of the diffraction pattern.

A set of scripts written in *Mathematica* by Lauer in this lab [45] simulates the propagation of radiation through a periodic index modulation or phase mask. *DiffUI.nb* in particular calculates the far field diffraction pattern of a finite plane wave propagated through a finite grating. The Fraunhofer approximation is assumed:

$$\frac{b^2}{\lambda \cdot z} << 1 \tag{2-8}$$

where b is the long dimension of the grating.

The calculations in *DiffUI.nb* assume a uniform, finite plane wave travelling through a same-sized finite grating. These conditions are approximated by the experimental setup for the diffraction measurement as described in Section 3.3 (Grating Characterization). The equations also assume that the grating is composed of regularly spaced columns of index change, constant throughout the thickness of the grating. This is an approximation of the gratings written by ultrafast laser. The index modulation is most likely more Gaussian than uniform through the cross-section. As well, the theory ignores the contributions of compaction and damage, such as voids, which may be present in the gratings and add scattered light. The effects of these approximations are discussed in Section 5.1.2 (Gratings).

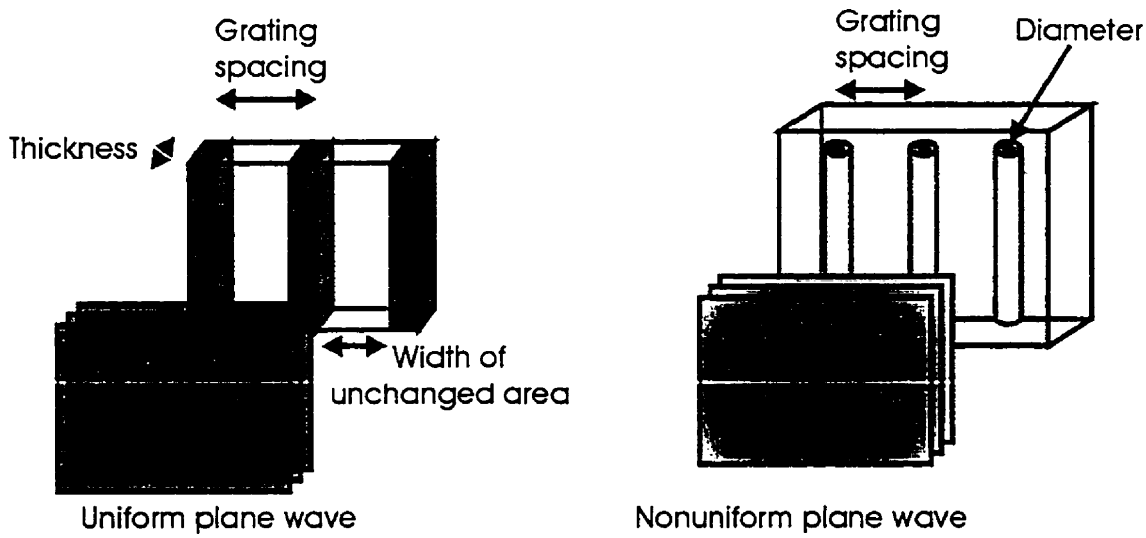

Figure 2-8 Figure of diffraction theory assumptions (left) compared to the real world (right). Assumptions are: finite wave on finite grating; perpendicular, uniform, plane incident wave; constant index change through the thickness; and regular grating width and spacing

Results from this script are plotted in Figure 2-9 under the parameter conditions of the gratings written for this thesis. This graph is used in Section 4.4 (Refractive Index Change Calculated from Numerical Aperture: Characterization of Waveguides) to determine the average index change of the laser-written cylinder from a diffraction efficiency (η) measurement, where η is the ratio of power in the first diffracted order to the power in the zeroth order.

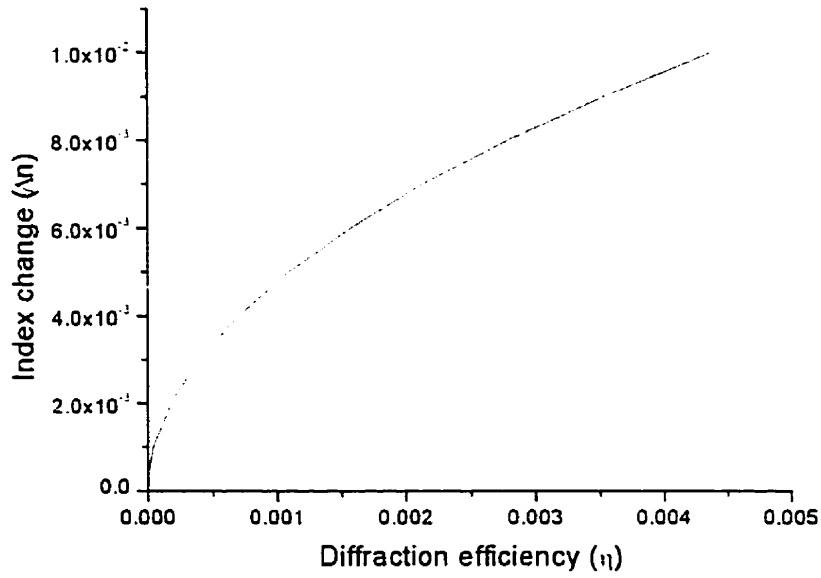

Figure 2-9 A graph of index change versus diffraction efficiency plotted from the output of *DiffUI.nb*. This graph is used to determine index change from measurements of diffraction efficiency from a grating.

Chapter 3

3 EXPERIMENTATION: SETUP AND METHODOLOGY

The aim of this thesis was to write index changes in glasses using an ultrafast laser. The first attempt involved the use of an Ar^+-pumped Mira Coherent (Ti:sapphire) laser in the University of Toronto Ultrafast Processing Lab. This was an unamplified system with an output of ~800 mW, ~120 fs pulses at 76 MHz. The laser was first converted from picosecond to femtosecond operation mode and then monitored for beam stability. A customized imaging and positioning system was then designed and built to write gratings in fused silica samples.

Though sparks suggesting plasma formation had been occasionally visible during writing, no visible diffraction pattern was discovered upon illumination with a probe laser. At pulse energies of ~10 nJ and a focal diameter of ~1 μm, the intensities reachable by this laser were ~9×10^{12} W/cm^2. Obara and coworkers had observed index modification at an intensity level of 1.5×10^{12} W/cm^2 with an amplified laser system. Mazur and coworkers, in using a comparable laser system to the Mira Coherent system, predicted a threshold at 25 nJ and a focal diameter of 0.5 μm, which is equivalent to an intensity of 8.1×10^{13} W/cm^2. Thus the Mira Coherent system, though producing no verifiable results, was most likely operating near the threshold for index modification.

The waveguides characterized in this thesis were written at the National Research Council (NRC) *Steacie Institute for Molecular Sciences, Femtosecond Laser Lab* 1[bc] in Ottawa. They were characterized at the University of Toronto Laser Processing Lab. The waveguides were characterized in a modified microscope-waveguide aligner system, with the placement of a CCD or power meter at various positions for different observations. The gratings were characterized using a laser illumination system and power meter detector. The following sections describe the processes of fabrication and waveguide characterization.

3.1 Waveguide and Grating Fabrication

The waveguides and gratings were written in fused silica and BK7 glasses. The samples were 0.5x0.5x2.0 cm^3, polished on the four larger surfaces. The working distance of the laser focussing objective (6 mm) limited the length of the waveguides, so they were written along the shorter length of the sample. The waveguides and gratings were written with the same experimental setup as described below. The gratings were simply composed of many parallel waveguides.

3.1.1 Experimental Setup

The ultrafast laser system used to write the index changes was partially home-built by NRC and consisted of a Ar^+-pumped Ti:sapphire oscillator, a stretcher, a regenerative amplifier (Coherent RegA 9050), and a single grating compressor. The output pulses had a maximum energy of ~1.5 μJ at 800 nm and a pulse width of 50 fs. The repetition rate could be varied with the maximum being 250 kHz. This provided the opportunity to study the effect of repetition rate on the writing process while maintaining constant fluence and

[b] Contact: Paul Corkum, (613) 993-7390, paul.corkum@nrc.ca

[c] Researcher: Andrei Naumov, GSI Lumonics

accumulated fluence (by adjusting scan speed to compensate). For the experiments described herein, repetition rates of 1, 10, and 100 kHz were applied.

A 10x microscope objective with 0.25 NA and a working distance of 6 mm focused the IR beam into the sample. The focused beam had a confocal beam parameter of ~17 μm and a beam waist diameter of ~3 μm.

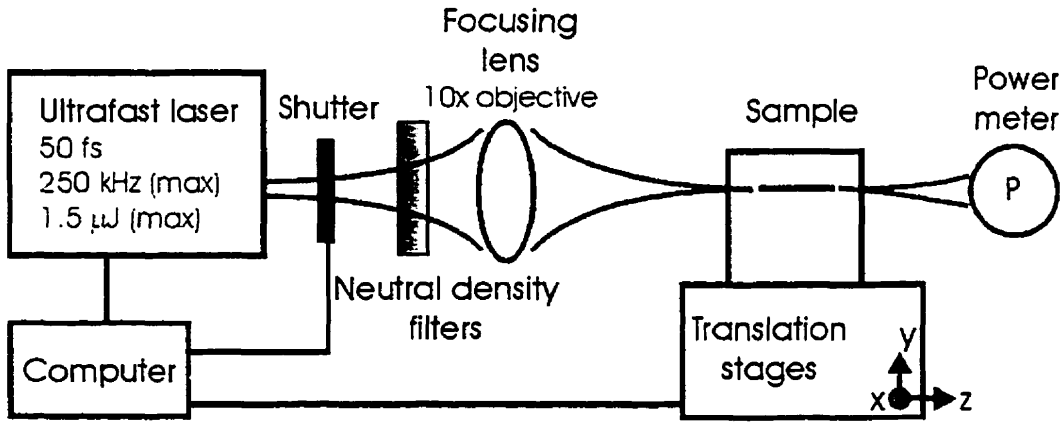

Figure 3-1 Ultrafast-laser optical-focusing system used to write waveguides and gratings at NRC.

The translation stage (Newport MM3300) moved in three dimensions, powered by stepper motors with 0.1-μm step size. Neutral density filters were placed in the path of the beam to control fluence, and a shutter in the path blocked the laser when necessary. Later, triggering of the laser was incorporated into the *LabView* program which controlled all the equipment during writing, and the shutter was removed. The ultrafast processing system is illustrated in Figure 3-1.

3.1.2 Mounting and Aligning the Sample

The glass sample was secured to a mount on a post. The post was attached to an xyz translation stage. The back reflection of the ultrafast laser from the sample surface was used to position the sample at a right angle to the laser beam axis.

A power meter was placed behind the sample to measure transmission power through the glass. This was used to monitor the transmission during laser exposure and to determine the position of the beam waist with respect to the surface of the sample before waveguide writing. Figure 3-2 is a sample transmission measurement, showing a decrease of ~90% when the waist penetrates the sample surface due to laser-matter interaction that decreases transparency.

The fluences used to write the waveguides exceed or are close to ablation threshold (~4.7 J/cm^2) and writing to the surfaces would not produce the pure index modifications at the ends of the waveguides necessary to effectively couple light in and out. So, it was necessary to precisely position (within ~50 μm) the beam waist relative to the sample surface to ensure that the waveguides began and ended ~150 μm within the sample. Waveguide lines were written at 50 μm intervals in depths in sample and then viewed under a microscope to determine which position had been closest to the sample surface.

The reference position corresponding to where the beam waist hits the sample surface, was then determined by correlating the visual results with the transmission measurements. The reference point was found to coincide with the minimum point of transmission.

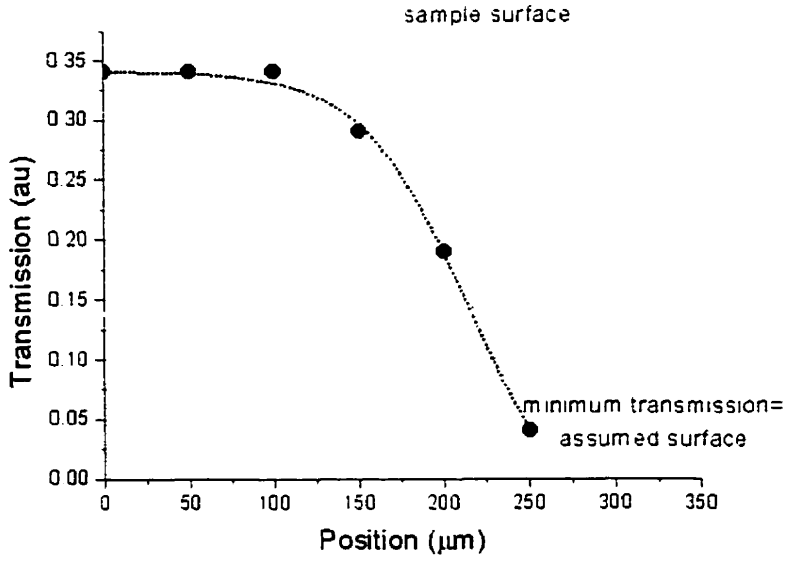

Figure 3-2 Transmission measurement of UF laser through glass sample. The lowest transmission point was used to align the beam waist with the sample surface.

3.1.3 Experimental Procedure

The first sets of waveguides (FSi.1 and BK7.6) were designed and written in the spring of 1999 at NRC by Naumov and Corkum [46]. *Visual Basic* programs controlled the laser and translation stages. Some details of the writing method are unknown to this laboratory, such as the sequence of instructions sent to the devices and the details of the instructions (e.g. whether the commands controlling the stages specified a translation distance or time). The waveguides were written in sets of three. Each set was written under the same system parameters, and the waveguides were spaced by 20 μm, with 30 μm among sets.

The parameters for the subsequent sets of waveguides were designed specifically for this thesis. The second sets of waveguides (Fsi.2 and BK7.1) were written by myself, M. Mehendale, and D. Coric. A *LabView* program was used to open the shutter, initiate translation of the stages at a set speed and for a set distance, reduced by a factor of n to account for the refractive index of the glass, and time the shutter to close. The

waveguides were written so that the sample moved axially towards the laser as depicted in Figure 3-1. The spacing between waveguides was increased to 50 μm to isolate light to one waveguide. The spacing between sets of waveguides was increased to 70 μm.

A subsequent set of waveguides (FSi.3) was written by Mehendale. System parameters were the unchanged from the set FSi.2, with the exception of the following: laser trigger control was added to the program, and the software was modified to start and stop triggering while the stages were in motion. This modification was necessary to ensure that the ends would not be subjected to more laser exposure than the rest of the waveguides. The waveguides were written so that the sample moved away from the laser in an attempt to determine whether the gross damage visible in the previous sets was dependent on this factor.

The gratings were also designed for this thesis and written by Mehendale. For this, the *LabView* program was altered to write a large number of "waveguides gratings" with a period of 12 μm. Failure of the Ar^+-pump for several months precluded the writing of further waveguide and grating samples.

3.1.4 Laser Processing Window

A major guide for the parameter range chosen for the waveguides was the work at Cornell University detailing refractive index modulations over a range of laser pulse energies (0.5-4 μm/s) and scan speeds (5-400 μm/s) [18]. Data taken from this paper was graphed in Figure 3-3 and Figure 3-4 as a surface plot, showing damaged points (**X**) and points for which the index modification was too small to be measured (**O**). A good quality processing area was interpolated with the damage and underexposed points as guidelines and is illustrated as dotted lines in the graphs below. At the top and bottom of the graphs, the boundaries define the high value and low fluence value limits respectively, beyond which

intensities induce damage or are insufficient to induce significant index modulation. At the left and right graph boundaries, the limitations are accumulated fluence rather than intensity.

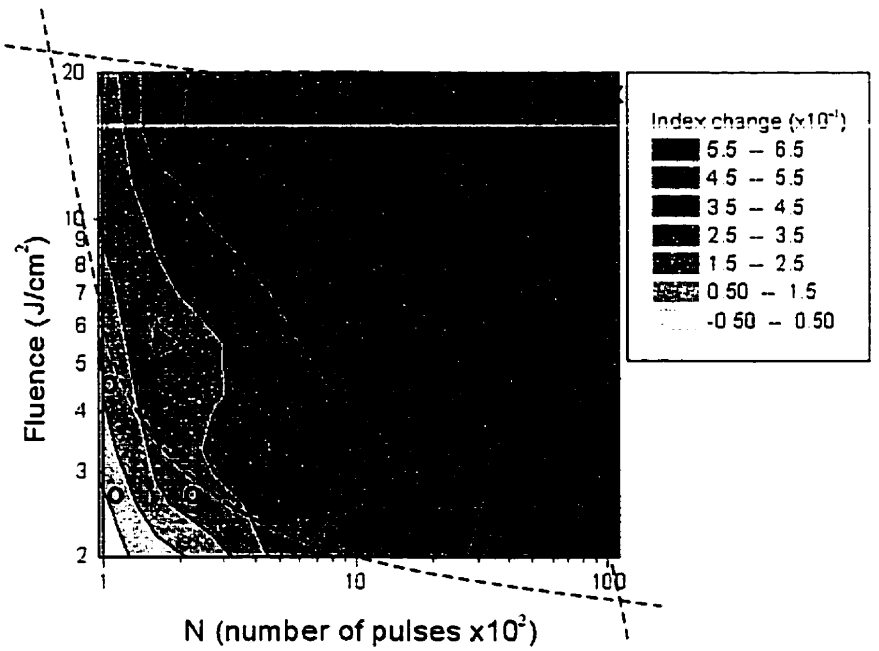

Figure 3-3 Parameter range for BK7, plotted from results of [18]. This plot is later used to choose laser processing parameters within the dotted lines. All results are at a repetition rate of 1 kHz.

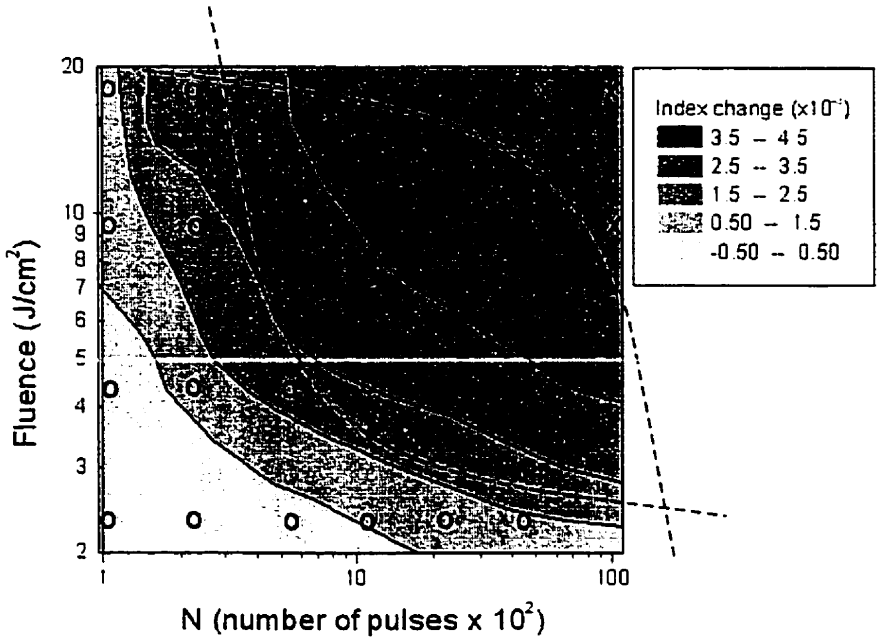

Figure 3-4 Parameter range for fused silica plotted from results of [18]. This plot is later used to choose laser processing parameters from within the dotted lines. All results are at a repetition rate of 1 kHz.

The laser-exposure parameters for writing waveguides were selected from the areas within the dotted lines in Figure 3-3 and Figure 3-4. Scan speed (5-200 μm/s) and repetition rate (1-100 kHz) were varied to adjust N, and energy per pulse (0.1-2 μJ) for fluence. Repetition rate was not varied in [18] and its effects would be difficult to demonstrate in contour plots such as above because it is incorporated into the variable N along with scan speed. This thesis explores the effects of varying this parameter and speaks to its effects in separate plots.

The energy per pulse was limited to a maximum of ~1.5 μJ/pulse from the laser and a minimum dictated by the sensitivity of the power meter (~0.1 μJ/pulse). The scan speed had an upper limit imposed by the desired accumulated fluence and a lower limit defined by a reasonable writing time. The repetition rate varied between the upper and lower limits of the laser as calculated from the range of desired accumulated fluence.

3.2 Waveguide Characterization

Waveguides were characterized by coupling light into one end and observing side scattered light and light exiting the waveguide on the other end. A fiber coupler xyz stage was adapted to a microscope for this purpose.

3.2.1 Microscope-Coupler System

The experimental setup used to characterize waveguides was a laser-diode coupled into a fiber and focused into the waveguides. The fiber and waveguides were mounted to precision xyz stages for alignment to optimize waveguide coupling. This positioning system was fixed to a microscope stage so that the microscope illumination source and objectives could be used to align and characterize the waveguides as shown in Figure 3-5.

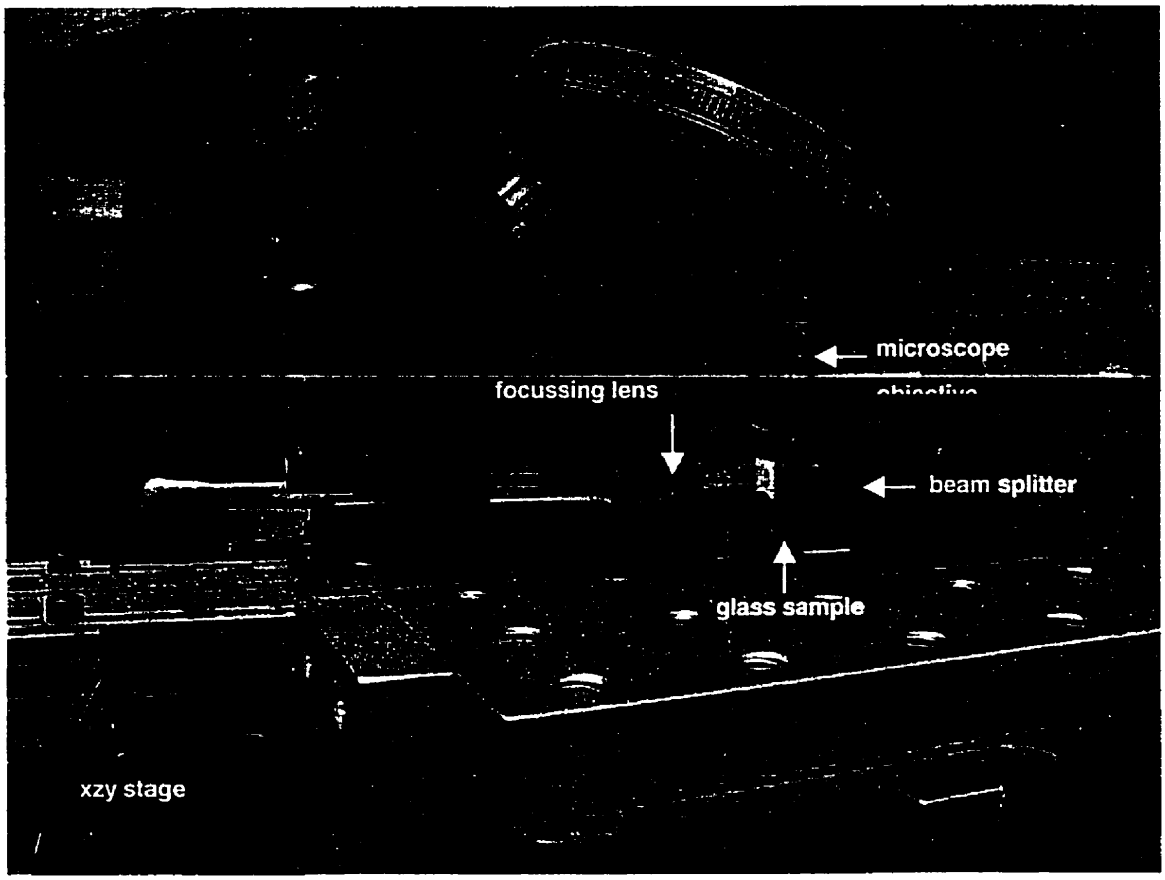

Figure 3-5 Photograph of experimental setup for coupling laser diode light into waveguides. The fiber from the diode laser appears on the bottom left. It is held in a brass chuck, which is held in a black adjustable chuck holder. A lens is fixed to the fiber chuck by a brass mount. The sample and beam splitter are fixed to the black tilt stage by a sample holder. All of these components sit on an aluminium breadboard, customized for this thesis, which is fixed to the microscope stage.

The diode laser system used to characterize the index changes in waveguides consisted of an AlGaInP laser diode (PDLD L63-312-0.5-PH6-1Fa). The output power of the diode laser was 5-mW. It emitted single mode CW light at 635 nm. The laser was connected to an FC/APC connector through a short section of single mode fiber (FS-SC-3224). The output from this fiber was ~0.8 mW.

A longer section of fiber (FS-SC-3224) was connected to the laser through an FC/APC connector. The other end of this long section of fiber was cleaved and polished and placed in a fiber chuck. The chuck was held in an adjustable fiber chuck holder (Melles Griot 17HFG 003) with pitch and yaw capability. This in turn was mounted on a precision

xyz stage (Thorlabs MDT602), giving the fiber five degrees of freedom to optimize coupling into the waveguides. A custom-made lens holder was mounted to the end of the fiber chuck. The output power after the lens was ~0.2 mW. The lens (Thorlabs 350230-B: 4.51 mm focal length, 0.55 NA) focused the laser light into the sample and could be positioned on the chuck to vary the NA (0.05-0.5) of the light entering the sample.

Figure 3-6 shows the sample and beam splitter mounted to a small tilt stage (Melles Griot 07TMT 505) with pitch and yaw positioning. The tilt stage was attached to an angle bracket and mounted onto a custom-made breadboard, which also held the Thorlabs xyz stage. This breadboard was fastened onto the microscope (Leitz Orthoplan 792300) stage so that controlled y- and z-translation of the sample was achieved by moving the stage. This permitted the field of view to be focused at a waveguide within the sample and along the length of a waveguide. Near-field viewing was facilitated through the microscope objective and far-field viewing by rotating the beam splitter 90° and projecting onto a screen. The sample could be translated in the x-direction by sliding in a rail over the stage, and could be fixed in an x-position by fastening the breadboard to the stage.

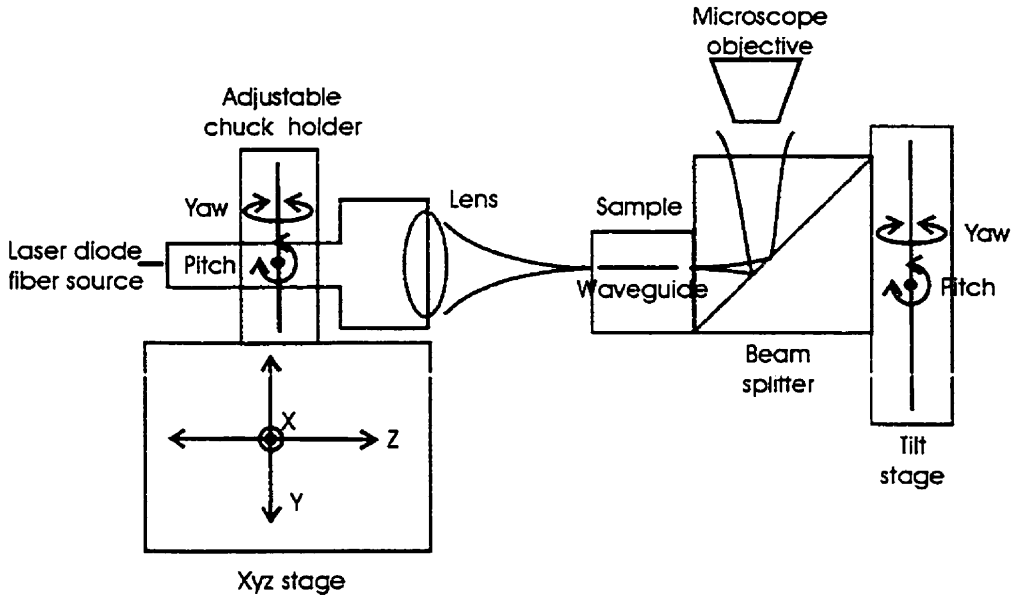

Figure 3-6 Experimental setup for characterization of waveguides, illustrating positioning features for sample and laser light source. Specifically, the xzy stage and adjustable chuck holder provide five degrees of freedom for the light source, and the tilt stage provides two degrees of freedom for the waveguide sample.

3.2.2 Coupling

The sample was mounted so that the waveguides were near the center of the tilt stage. It was held in place with a component holder. Once in place, the sample was aligned with the axes of the microscope stage through adjustment of the two thumbscrews on the tilt stage.

The NA of the laser light from the focussing lens was initially set to ~0.05, a value calculated from the expected index modulation value of 0.001. It was varied to attempt maximum coupling and finally set to 0.10. This value matches the higher index waveguides quite well and slightly overfills the weaker waveguides.

The fiber was coarsely aligned in the x-direction (as defined in Figure 3-6) by viewing through the microscope. It was aligned in the y-direction (as defined in Figure 3-6) by translating a known distance from the top edge of the sample. And it was aligned in the z-(waveguide axis) direction by viewing the front end of the waveguide through the beam

splitter. The microscope view was imaged onto the front end of a waveguide by illuminating the waveguides from that end with a fiber scope, as illustrated in Figure 3-7. Then the white light was turned off and the diode laser turned on. The fiber was translated along the z-axis until the smallest spot size was observed and the beam waist then coincided with the beginning of the waveguide.

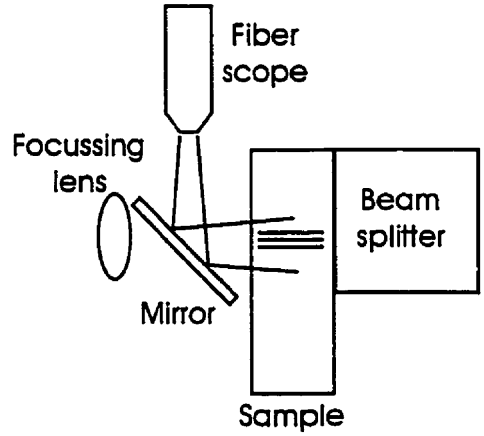

Figure 3-7 A top view of the experimental setup used to illuminate waveguides from the front ends. This allowed the ends of the waveguides to be visible from the ends so that the beam waist could be overlaid.

The xyz-position and pitch and yaw of the fiber light source were then adjusted to improve coupling. Three criteria were used, in this order, to optimize coupling:

1. The far field pattern, as projected onto a screen behind the sample, produced an interference pattern of rings. A CCD image of this pattern is visible in Figure 3-8.
2. The amount of side scattered light, as observed from the side by eye (see Figure 3-9) and from the top through the microscope (see Figure 3-10), was maximized.
3. The amount of light exiting the waveguide, as viewed through the microscope focused onto the end of the waveguide through the beam splitter, was maximized. Figure 3-11schematically depicts the configuration for this measurement.

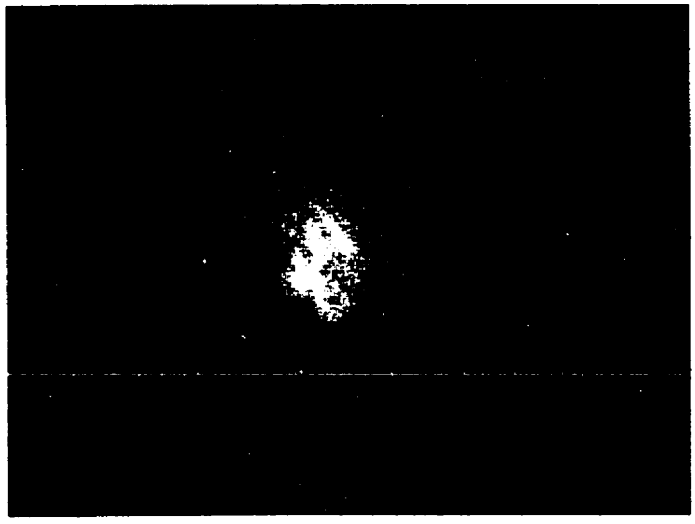

Figure 3-8 The far-field interference pattern of light coupled and uncoupled in the waveguides. The rings are visible only when light is coupled into the waveguide.

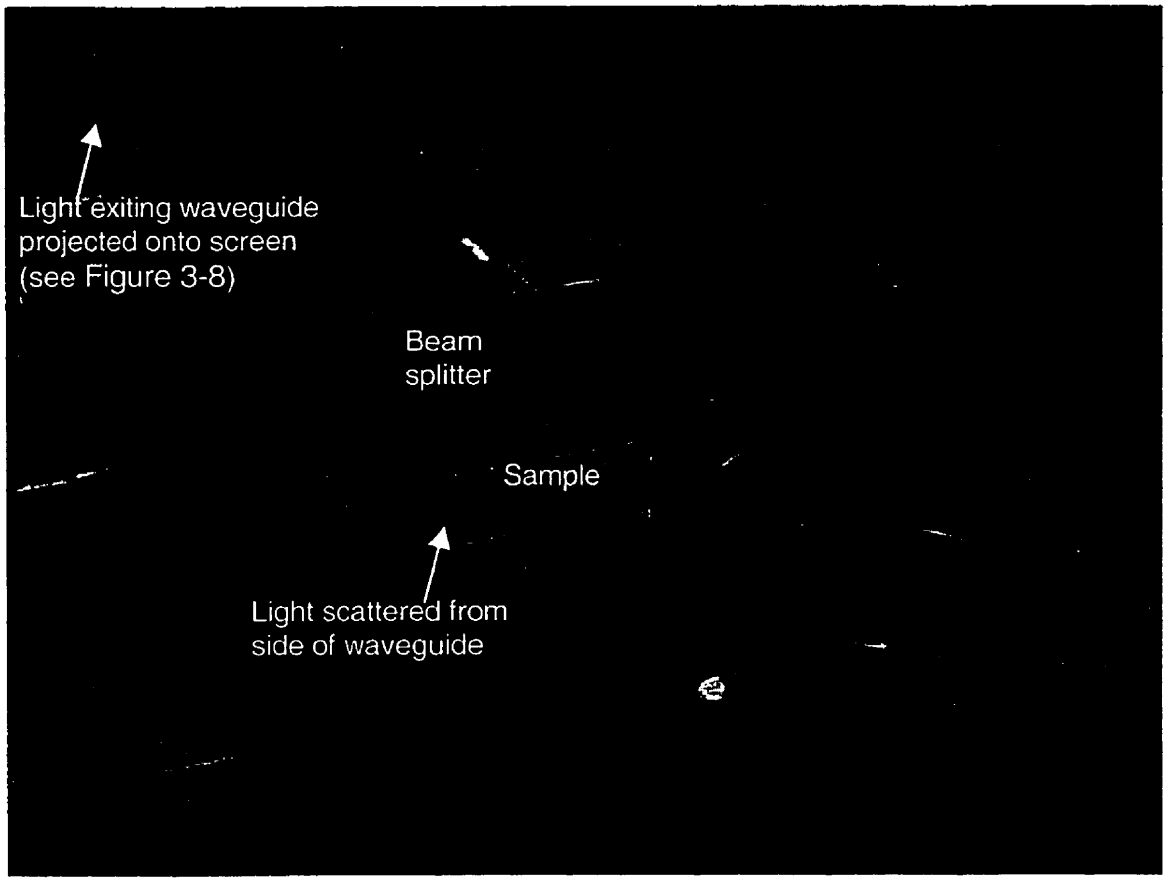

Figure 3-9 Photograph of coupling setup. Light scattered from the waveguide is visible by eye in a dark room and is a visual means of confirming coupling, along with the rings visible on the far screen.

3.2.3 Scattered Light

Waveguides losses were measured by recording scattering of coupled waveguide light from the sides of waveguides with two devices: a charge coupled device (CCD) camera and a power meter. A slit made from razor blades was placed at the image plane of the 32x microscope objective inside a 10x eyepiece to filter out light not originating from the waveguides. The microscope stage was translated horizontally to align the waveguide with the slit. The experimental system for this measurement is shown in Figure 3-10.

A CCD camera (Panasonic GP-K2205) connected to a PowerMac using Apple Video software captured images through the eyepiece at the top of the microscope. *NIH Scion* software was used to calculate the intensity profiles along the axis of the waveguide for an estimate of the loss per distance.

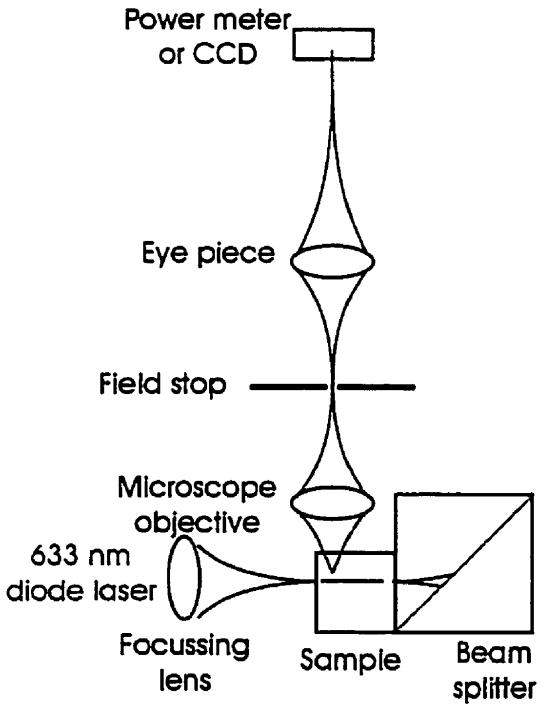

Figure 3-10 Experimental arrangement for measuring scattering losses from bulk waveguides. Translation of the sample allowed measurements of loss to be taken along the length of the waveguide.

Due to insufficient sensitivity of the CCD, the light scattered over the whole length of the waveguides could not be recorded. Moreover, the waveguides were short (~4.5 mm) and the calculated loss per distance figures must be used with discretion. For good quality waveguides, the amount of scattered light was undetectable by eye, CCD, or power meter and so there are no loss measurements for them.

An optical power meter (Newport 1830-C) was also positioned at the top of the microscope eyepiece to measure scattering losses. The readings fell quickly to the noise level (10 pW) within the first millimeter of the waveguide. Large coupling losses at the beginning of the waveguides and the short length of the waveguides themselves made it very difficult to measure loss per distance. As well, the resolution of such measurements was hindered by the periodic scattering defects along laser-damaged waveguides, which inserted large section-to-section variations in power measurements. However, by capturing light over the length of the waveguide, total scattering losses were estimated.

3.2.4 Numerical Aperture

The CCD camera was also used to capture images of the diverging light from the waveguide end as shown in Figure 3-11. Light exiting a waveguide was collected by a microscope objective (32x magnification, 0.30 N.A.), along with the fiber laser diode light that had not been coupled into the waveguide. The objective focused this light onto an image plan below the eyepiece lens at the top of the microscope. A pinhole placed at this image plane acted as a spatial filter permitting only the light that had exited the waveguide to pass through. Light which had not been coupled into the waveguide would not have passed through the pinhole as it would have been out of focus at this plane, having originated from a further distance than the waveguide-coupled light. With the eyepiece lens removed, the light that passed through the pinhole continued to diverge, and its

cross-section was captured on the CCD ~6 cm away, providinng a far-field image. The half-width at half maximum (HWHM) of this image is used to calculate the NA of the beam, $NA_{atPinhole}$, which is related to the NA of the waveguide, N_{wav}, by the magnification of the microscope objective:

$$NA_{wav} = 32 \cdot NA_{atCCD} \tag{3-1}$$

for the 32x microscope objective.

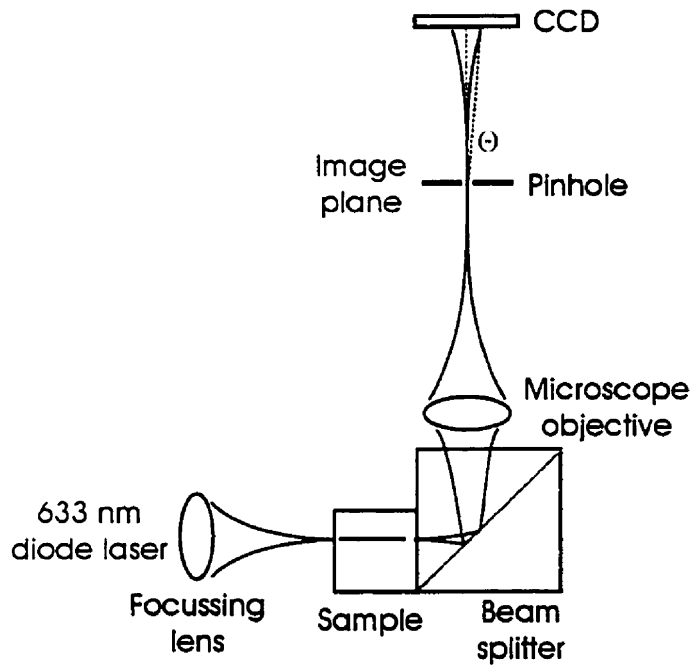

Figure 3-11 Experimental setup for measuring the numerical aperture NA_{wav} of light coupled to ultrafast laser-written bulk waveguides. SinΘ is the NA of the magnified beam, from which the NA of the waveguide can be determined.

3.2.5 Transmitted Light

The same setup used for the measurement of NA was also used to measure the transmitted power of the waveguides. In this case, a power meter replaced the CCD camera. The transmitted and scattered light powers were compared with the input power to estimate coupling efficiency. The experimental system for this measurement is shown in Figure 3-11.

The laser diode was unstable (dropping ~75% in one hour) and the output power from the fiber was reset to 125 μW, by adjustment of the current, before every measurement. When the required current exceeded the maximum operating range, the laser was shut off for cooling.

3.3 Grating Characterization

The helium neon (HeNe) laser system used to characterize the gratings consisted of a 5-mW HeNe laser (Uniphase 1507G0), a spatial filter, a collimating lens, and an aperture before the sample as shown in Figure 3-13. The HeNe laser produced a Gaussian beam, which did not match the theoretical conditions described in Section 2.5.2 (Gratings). The remaining elements described in this paragraph cleaned up and modified the HeNe output to better meet the assumptions of the theory. The spatial filter eliminated the noise. It consisted of a 40x, 0.65 NA microscope objective, which Fourier-transformed the HeNe output to a spatial mapping of its frequency components. This projected the higher frequency noise into rings surrounding a clean central Gaussian beam. The beam was focused through a 1 mm x 1 mm pinhole, matching the grating dimensions, which removed the noise component of the beam. The diverging beam was then collimated by a lens to approximate a plane wave, and sent through an aperture ~1.5 cm in diameter, which selected an area of the beam with minimal intensity variation to approximate a uniform, finite beam.

Five grating areas had been written in a fused silica sample, spaced apart by 0.5 mm. The sample was first positioned so that the HeNe light was on the edge of the sample where the gratings began. It was then translated in the y direction across the gratings until a diffraction pattern could be seen. This pattern was optimized by translation in the x and

y directions until the first order diffraction peak yielded maximum power as measured by a power meter.

A second aperture, placed ~20 cm behind the sample on xy-stages, isolated the zero or first diffraction orders for measurement by a power meter place ~10 cm from the aperture. The aperture position was optimized by power meter detection of one of the diffraction orders.

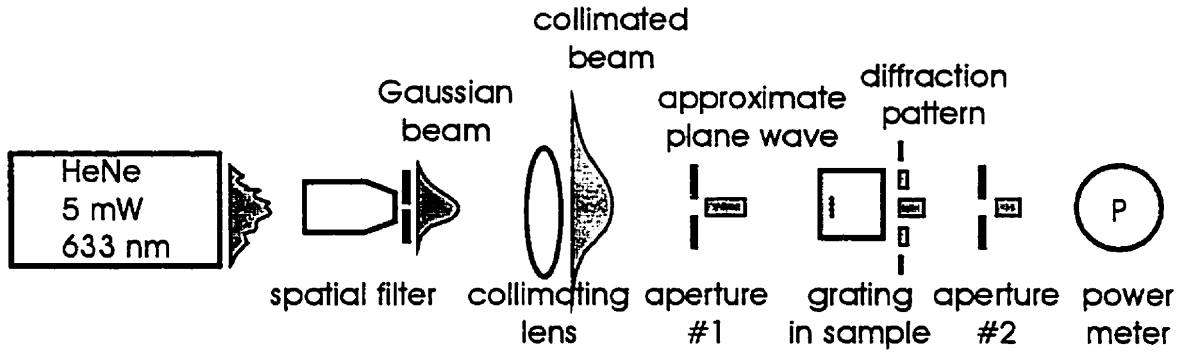

Figure 3-12 Experimental setup for measuring the diffraction efficiency of gratings. The spatial filter, collimating lens, and first aperture modify the Gaussian beam to approximate the theoretical assumptions of a plane uniform wave.

Measurements of subsequent gratings were made by x-translation of the sample until a new diffraction pattern was visible. The transition between gratings was sufficiently clear, with two dim patterns visible concurrently when the HeNe overlapped both gratings.

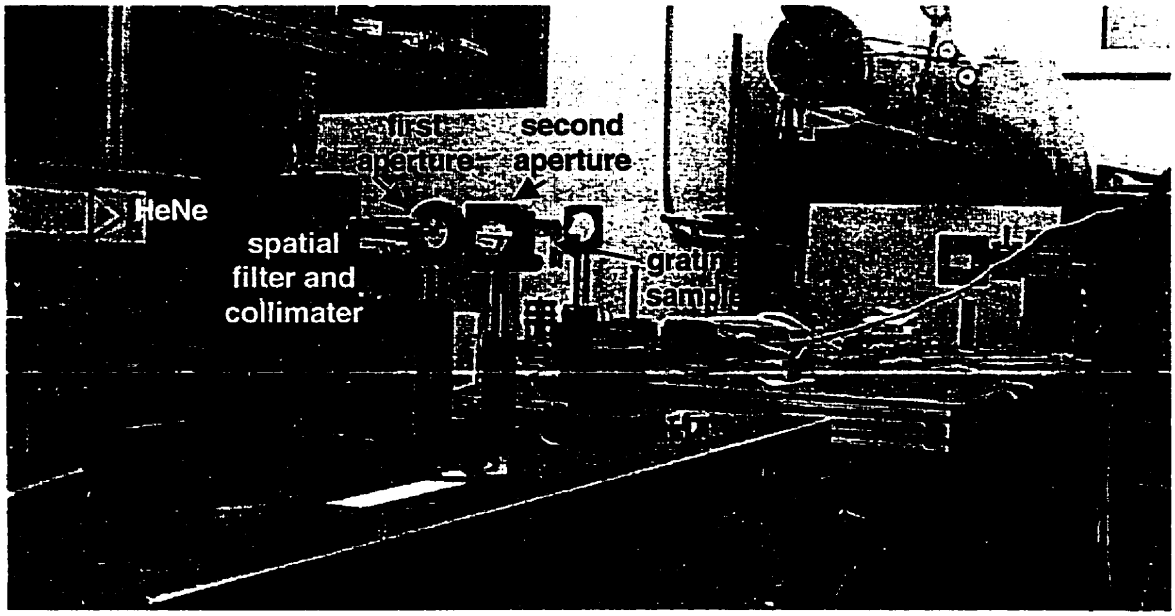

Figure 3-13 Experimental setup for characterization of gratings by examination of diffraction pattern. A HeNe is visible on the far left. It is directed at a spatial filter, collimating lens, aperture, and sample holder. The second aperture sits on the far end of the table.

Chapter 4

4 RESULTS

4.1 Visual Observations

Many of the laser writing parameters could be coarsely inferred simply by viewing the waveguides under the microscope with white light. For example, waveguides written in fused silica at high repetition rate (100 kHz) and high laser energy (> 1 μJ) had obvious periodic damage along the length of the waveguide. At a lower repetition rate (10 kHz), the damage was less pronounced and its period appeared smaller. This was sometimes helpful in verifying the laser writing parameters and gaining an intuitive insight into the processing window for good quality waveguides.

4.1.1 Material Effects

Waveguides were written in both fused silica and BK7 samples. Waveguide-coupled light could not be observed from the BK7 waveguides and so they were not studied in depth (see Section 5.2.1 (Comparison with Cornell University)). Sections 4.2 to 4.5 discuss results obtained solely from fused silica samples. However, visual observations initially suggested that BK7 would have been a better material for laser writing of waveguides. As can be seen in Figure 4-1, ultrafast-laser modification of BK7 did not result in the same periodic damage seen in fused silica samples; the waveguides are much smoother.

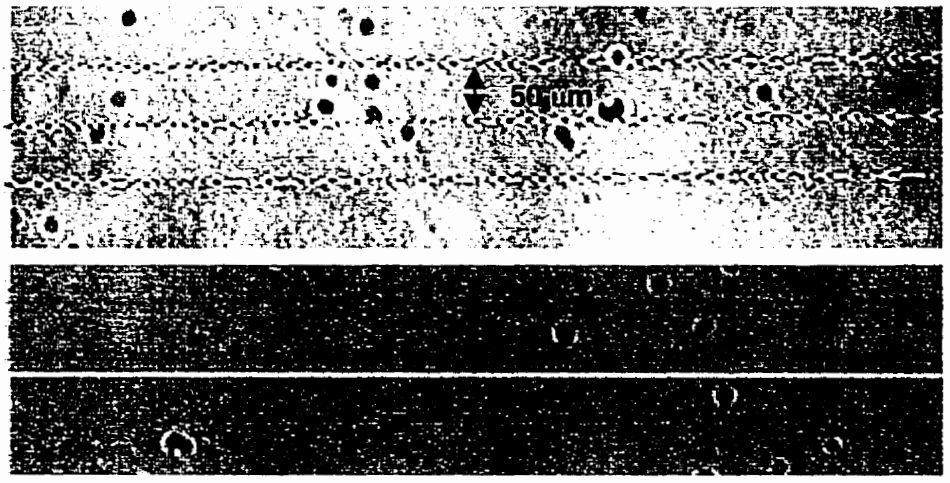

Figure 4-1 CCD camera image of fused silica (top) and BK7 (bottom) waveguides written with ~1 µJ pulses at 200 µm/s and 100 kHz repetition rate. The fused silica sample waveguides have more visible damage.

4.1.2 Parameter Effects

Certain laser exposure parameters appear to play an important role in the optical quality of the laser-written waveguides. Waveguide visibility by white-light backlighting is highly dependent on the repetition rate, and to a slightly lesser extent, the pulse energy at which the waveguides were written.

The waveguides written at 10 kHz are less visible than those written at 100 kHz, with fewer severely damaged regions (see Figure 4-2). Waveguides written at 1 kHz are not visible at the magnifications possible with this system (< 32x).

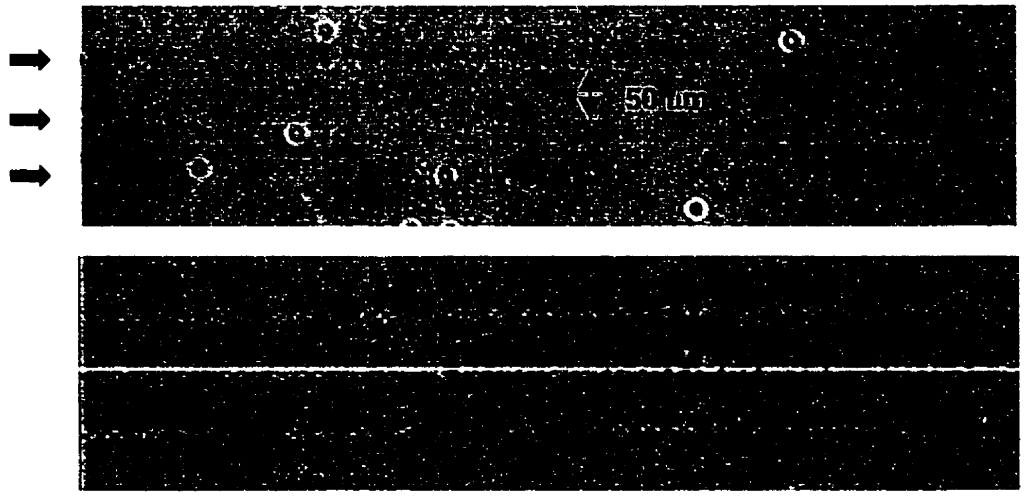

Figure 4-2 The effect of repetition rate on visibility of damage is seen by comparing fused silica waveguides written at the same fluence and accumulated fluence. The top set at 10 kHz and 20 μm/s show less damage and the bottom set at 100 kHz and 200 μm/s show more visible damage.

Longitundinal intensity profiles of the CCD images of waveguides in Figure 4-2 reveal damage at comparable periodic intervals (~2 μm) for the different repetition rates. However, at 100-kHz rates, there exists more pronounced damage at larger periodic intervals (~ 7 μm) (see Figure 4-3). This may be attributed to two factors: the instability of faster scan speeds, required with higher repetition rates to maintain similar accumulated fluences; and the smaller thermal transport distances for 100 versus 10 kHz repetition rates. These are both further discussed later in Section 5.1.1 (Ultrafast Laser-Written Waveguides: Defining a Processing Window).

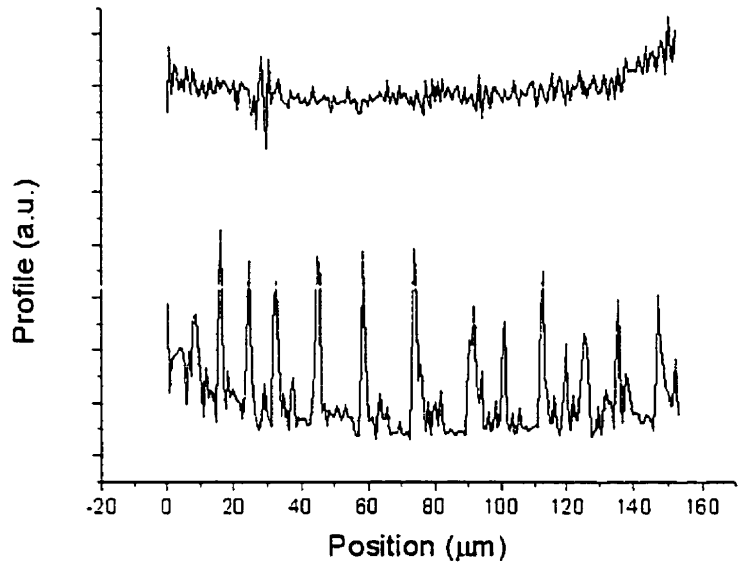

Figure 4-3 Profiles of CCD camera images of the waveguides in **Figure 4-2** written in fused silica at 10 kHz (top) and 100 kHz (bottom) with 1 μJ pulses. Periodic peaks correspond to periodic visible damage along the waveguides.

The waveguides written at the lower energy of 0.2 μJ are less visible and are less damaged as can be seen in Figure 4-4.

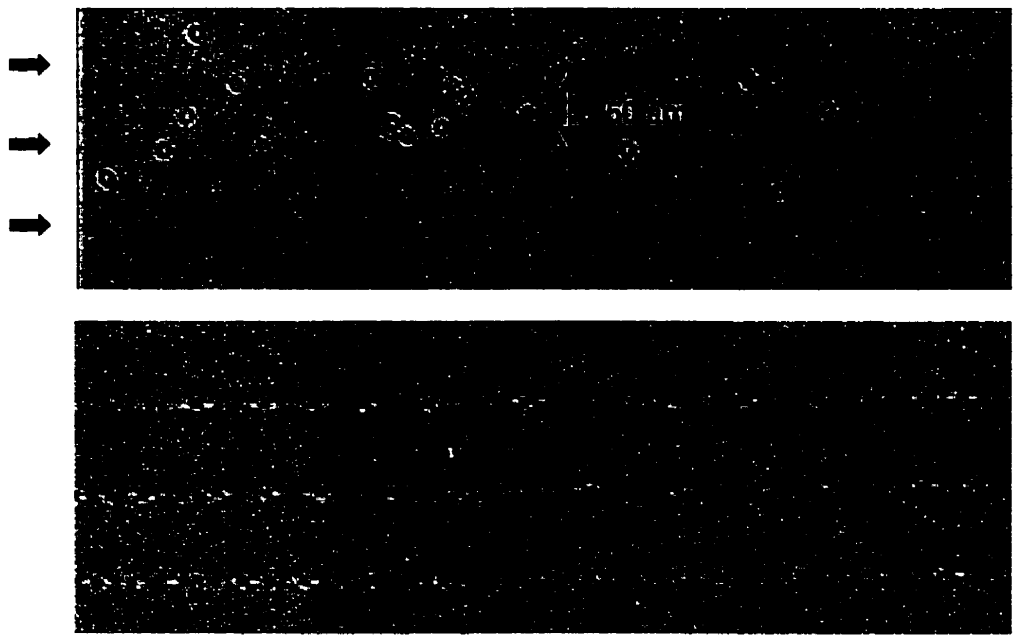

Figure 4-4 The effect of pulse energy on visibility of damage is seen by comparing fused silica waveguides written at the same repetition rate (100 kHz) and scan speed (100 μm/s). The top set were written at ~0.5 μJ and the bottom ones at ~1 μJ.

4.2 Waveguide Scattering Losses

Scattering losses are due to guided light reflecting or refracting from damage (localized index variations and voids) and variations in cross-sectional diameter in the waveguides. The waveguides written at a lower repetition rate (10 kHz) did not scatter enough light to be detectable by human eye, CCD camera, or power meter. These constituted low-loss and good quality waveguides. Only scattering losses from waveguides written at higher repetition rates (10 kHz) were measurable.

CCD images of scattered light from waveguides were used to determine waveguide loss per distance. Losses result from absorption and scattering. The relative amount of light scattered out of the waveguide is a constant percentage of the waveguiding light power and thus a measure of the amount of guided light. The difference in intensity along the length of the waveguide divided by the length of the waveguide is a measure of the dB-loss per distance.

The intensity data of the CCD camera images was spatially filtered to remove the highly scattered light from the periodic defects of the waveguides, and the loss was determined from a linear fit of the baseline data. Figure 4-3 is the plot of the log of the intensity data and the linear fit is used to estimate the scattering losses. Losses were only determined for the highly scattering waveguides written at 100 kHz repetition rate because the quantity of scattered light was insufficient for measurement in the remaining better-quality waveguides. The measured losses were in the range of ~4 dB/cm when written with 2 μJ/pulse and <1 dB/cm when written at 0.2 μJ/pulse. Note that these values apply to the waveguides that scatter the most light and therefore are the most damaged.

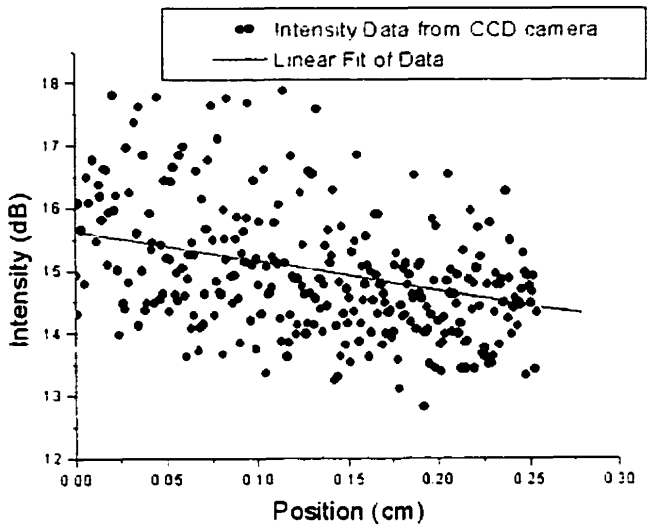

Figure 4-5 Intensity profile from CCD camera image of scattered light from a waveguide written with 2 μJ/pulse, 100 kHz, 200 μm/s scan speed. The intensity values are on a log scale and the linear fit is a dB loss per centimeter of the scattering losses of the waveguide.

Measurements of scattering power losses by the power meter were used to estimate the total waveguide scattering losses (L_{total}) by the following formula:

$$L_{total} = P\frac{2\pi}{2\cdot\sin^{-1}(NA)} \tag{4-1}$$

where P is the power of the scattered light collected by the 10x, 0.22 NA microscope objective. Absorption of light by the lenses is ignored here.

Results of the 100 kHz repetition rate waveguides indicate that the slower scan speeds of 50 and 10 μm/s, versus higher speeds of 100 and 200 μm/s, produced waveguides with less scattering losses: ~3 μW versus ~ 10 μW. This is consistent with optical microscope observations of the scattered light, which is dimmer and more uniform for the more slowly written waveguides. Scattering was less pronounced for the 10 kHz repetition rate waveguides. Relatively more light was also noted to scatter from the far end of the

waveguides rather than the end closer to the laser source. This might perhaps have been due to extremely poor coupling at the front end and Fresnel reflection at the other end.

4.3 Waveguide Transmission

Total waveguide transmission power is affected by both coupling and scattering losses. Figure 4-6 plots the waveguide transmission power as a function of the number of pulses. The effect of pulse energy (fluence) and scan speed is depicted.

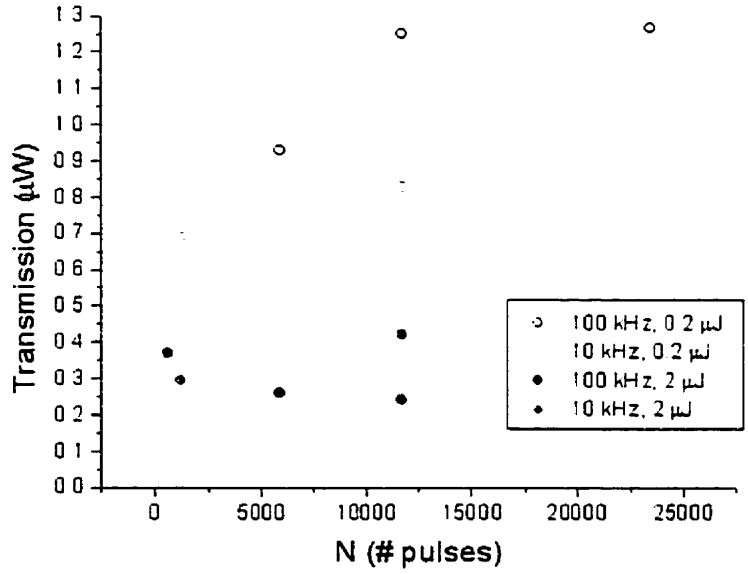

Figure 4-6 Plot of waveguide transmission power at a fixed input power of 125 μW, plotted against exposure (number of pulses) for waveguides written in fused silica. A lower energy per pulse writing beam results in waveguides with higher transmitted power.

The waveguides with the lowest transmission were written at the higher laser energy of 2 μJ. This is most likely due to damage at higher laser energies and therefore scatter more light. The waveguides with the highest transmissions were written at low energies values and low scan speeds values. The higher repetition rate of 100 kHz also appeared to produce a more transmissive waveguide.

Coupling efficiency (η_c) can be estimated with the knowledge of transmission (P_{out}) and scattering (L_{scat}) powers:

$$L_{coupl} + L_{abs} = P_{in} - L_{scat} - \frac{P_{out}}{0.5 \cdot 0.96^n} \tag{4-2}$$

where P_{in} is the power of the light after the focussing lens (125 μW). The measure of transmitted light P_{out} must be divided by a factor of 0.5 to account for the beam splitter and 0.96^n for the Fresnel losses where n is the number of lens interfaces. Absorption loses L_{abs} are considered insignificant.

Only the high-energy laser-written waveguides yielded scattering power loss data, producing power loss values that exceeded the total power transmission as depicted in Figure 4-6. Thus the majority of light coupled into these waveguides was scattered out. The coupling efficiency is ~ 10% as determined by the ratio of L_{coupl} to P_{in}. The maximum scattered light from the low-energy waveguides was 1 μW (as calculated from the detection limit of power meter), which is comparable to the amount of transmitted light. The coupling efficiency in this case is ~ 4%. This poor coupling could be due to a NA mismatch that results from coupling being better optimized previously for the waveguides formed with higher laser energy.

4.4 Refractive Index Change Calculated from Numerical Aperture: Characterization of Waveguides

Figure 4-7 plots the laser-induced refractive index modulation as a function of accumulated fluence (F_{acc}), which is defined as:

$$F_{acc} = N \cdot F = \frac{r \cdot b \cdot U}{v \cdot A} \tag{4-3}$$

where N is the number of pulses, F is the fluence, v is the sample scan speed, r is the laser repetition rate, U is the energy per pulse, and A is the focal area (½ intensity). The confocal beam parameter (~17 μm), b, his found from the equation:

$$b = \frac{2\pi \cdot w_o}{\lambda} \tag{4-4}$$

where w_o is the beam waist radius, and λ is the laser wavelength.

The plot in Figure 4-7 shows a possible dependency of index change on pulse energy and repetition rate. The high pulse energy of 2 μJ (open circles) causes more damage, as was discussed in Section 4.1.2 (Parameter Effects). The three highest accumulated fluence points (> 100,000 J/cm^2) are most likely too damaged for precise NA measurements. The lower pulse energies (solid circles) result in more consistent NA measurements, giving index modulations in the range of 0.002 to 0.004. Higher index modulations are achieved at the higher repetition rate.

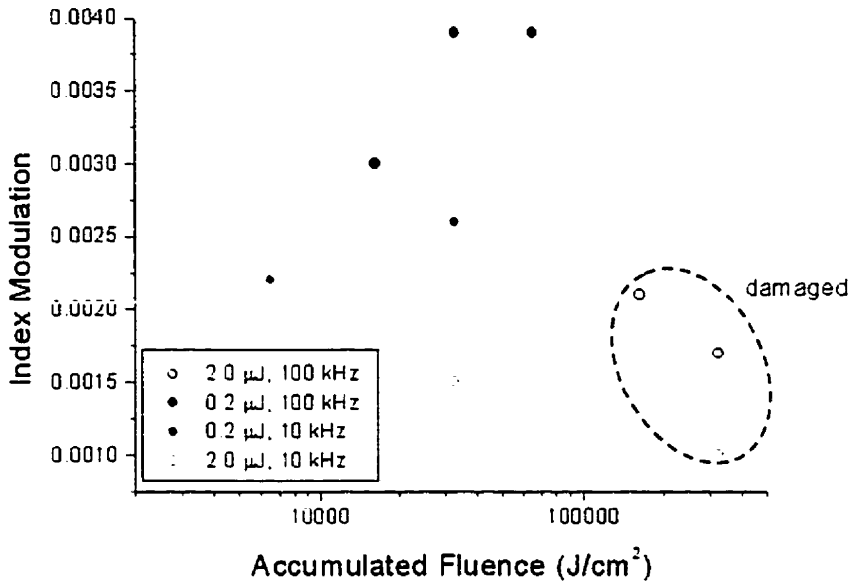

Figure 4-7 Plot of index modulation in fused silica versus accumulated fluence. The three points above 100,000 J/cm^2 are most likely damaged by overexposure.

4.5 Refractive Index Change Calculated from Diffraction Efficiency: Measurement of Gratings

Five gratings were written to provide index modification measurements for comparison with the NA of waveguides method. The parameters of the gratings were selected such that the writing of each grating area could be completed in a reasonable time of less than thirty minutes. This limited the scan speed to be greater than 100 μm/s. All variables (scan speed, repetition rate, and pulse energy) were explored and parameter values were chosen from within the processing area shown in Figure 3-3 and Figure 3-4. The final parameters are given in Table 4-1.

The grating areas were 1 mm x 1mm, with a period of 12 μm. The highest diffraction efficiency would have been produced with gratings of period equal to twice the grating thickness. However, this value would double the required grating writing time. The

waveguide grating diameter here is taken as the diameter of the beam waist (3 μm). Visual observation under microscope confirms that the diameter of the waveguide gratings is approximately 3 μm with an error of up to 1 μm due to unclear boundaries. This leads to errors of up to 100% error in the index change.

The three gratings written at higher energy (1.0 μJ/pulse) produced clear diffraction patterns with three to five orders discernable by eye. Their index modulations, as taken from **Figure 2-9**, are summarized in Table 4-1. No diffraction patterns were visible from the gratings written at lower energy (0.2 μJ/pulse).

Table 4-1 Summary of refractive index modulations for the ultrafast laser-written gratings.

Repetition Rate (kHz)	Scan speed (μm/s)	Diffraction efficiency (η)	Index modulation (Δn)
100	100	0.0042	9.7×10^{-3}
100	200	0.0032	8.5×10^{-3}
10	100	0.0030	8.2×10^{-3}

Chapter 5

5 DISCUSSION

The results of this thesis work help to define a new processing window by the exploration of new laser processing parameters for defining intricate patterns of refractive index inside optical glasses. The most distinctive parameter is repetition rate. Difficulties with the characterization of waveguides prompted the writing of volume gratings for comparison of index change measurements. Comparisons and contrasts of general ultrafast-laser results with other laser-processes in the UV spectrum provide a useful reference and reinforce the effects of repetition rate.

5.1 Summary of Results

5.1.1 Ultrafast Laser-Written Waveguides: Defining a Processing Window

Two noteworthy inferences that can be drawn from the results of this thesis are the effect of repetition rate and scan speed to the optical quality of waveguides. As was noted in Section 4.2 (Waveguide Scattering Losses), waveguides written at slower speeds (< 50 μm/s) transmit light better. It is possible that the stepper motors controlling the stages do not move smoothly at high speeds. Alternatively, there is the advantage of a greater overlap of the beam spot when the laser focal volume moves more slowly through the sample (99.994% at 10 μm/s vs. 99.94% at 100 μm/s between pulses at 10-kHz repetition

rate). Slow speed and high repetition rate further offer a thermal treating of the laser-interaction volume for improved processing, as is discussed below.

The second processing variable affecting the waveguides was the repetition rate. Higher repetition rate (100 kHz), at higher energy (2 μJ/pulse), induced larger damage sites, while lower energy (0.2 μJ/pulse), produced larger index modulations and fewer damage sites. Clearly, higher laser energy, at high repetition rate is damaging, exposing the material to excessive accumulated fluences. However, at lower energy, high repetition rates may provide an advantage in terms of heat transport, as will be discussed in Section 5.2.1 (Comparison with Cornell University). The thermal-diffusion scale length at 100 kHz repetition rate is ~6 μm, versus ~18 μm and ~60 μm for 10 kHz and 1 kHz rates, respectively. At 100 kHz, a thermal component remains in the processing volume as subsequent pulses arrive, which allows the material to be more ductile and less conducive to micro-crack formation [12].

This thesis has also begun to map the processing window for index modification in fused silica by ultrafast lasers up to a repetition rate of 100 kHz. Figure 5-1 are contour plots of index change as a function of fluence and number of pulses. They illustrate portions of the processing windows at 10 kHz (left) and 100 kHz (right). Upper fluence limits and "number of pulse" boundaries are visible on the top and right boundaries of the graph respectively as identified by the damage points (**X**). Additional data is required to more accurately define these boundaries. The values superimposed on the contour plots are index change measurements $x10^{-3}$ and the contours are interpolated from the data.

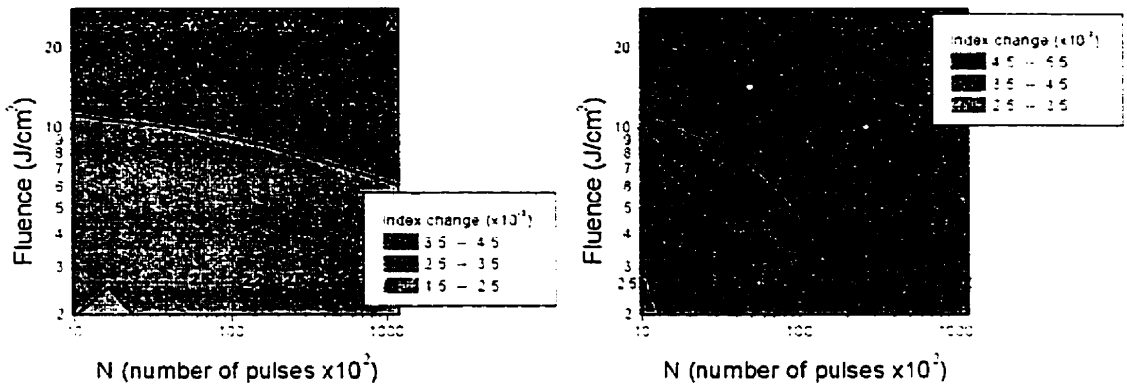

Figure 5-1 Map of processing window for ultrafast-laser induced index modification of fused silica at 10 kHz (left) and 100 kHz (right) repetition rate. **X** represents damaged waveguides from which no index change measurement could be taken.

Lower fluence and "number of pulses" limits are not visible due to lack of data in the lower range. The amount of data collected was limited to the first sample of waveguides (FSi.1) because of poor coupling into subsequent samples. These cursory results show that the higher repetition rates of 10 kHz and 100 kHz will induce higher index changes than a lower repetition rate of 1 kHz under the same fluence and number of pulses (i.e. compared with FIG GAETA). For example, at ~10^4 pulses and ~2.5 J/cm^2 fluence, 100 kHz repetition rates will induce an index change of ~3.9×10^{-3} (taken from Figure 5-1 right), versus ~2.5×10^{-3} at 10 kHz (from Figure 5-1 left), versus ~1×10^{-3} at 1 kHz [18]. A four-fold scaling of refractive index change appears possible with scaling from 1-kHz to 100-kHz repetition rate.

The scarcity of data was due not only to lack of access to a laser system, but also several technical issues that prevented all the written waveguides from being characterized. Section 3.1.3 (Experimental Procedure) mentioned attempts to explore ultrafast-laser waveguide-writing conditions, specifically variation of scan direction, timing of system components, and waveguide spacing.

Our collaborator, Corkum, proposed that scanning in the backward direction (sample moves away from laser) versus forward direction (sample moves towards laser) would improve the quality of the waveguides by allowing the laser to back away from any thermal region or plasma rather than propagating through such sections. However, waveguides written in both manners did not exhibit noticeably different visible damage or transmission.

There was difficulty in coupling light out of the second sample of waveguides (FSi.2) and an attempt was made to modify the writing of the ends of the waveguides to avoid damage due to overexposure. Rather than using a shutter to turn the laser on and off synchronously with the starting and stopping of the sample scanning, the laser was triggered on and off while the sample was in motion. This latter method preventing overexposure due to mis-timing synchronization and/or acceleration of the sample motor drives. The third sample of waveguides (FSi.3) was written using this new method of controlling the laser exposure. This procedure did not seem to significantly improve the optical coupling; however, there were other irregularities in this set of waveguides that may have contributed to their poor quality. Specifically, the waveguides were of irregular lengths and varied in the extent of damage along its length.

Finally, there was difficulty confining light to one waveguide in the first set of waveguides. Many of the waveguides in sample FSi.1 were damaged due to overexposure. This may have induced stresses into the inter-waveguide regions. The waveguides were spaced apart by only 20 μm in this sample and by increasing the spacing to 50 μm in subsequent samples, this problem was eliminated.

5.1.2 Gratings: Verifying Index Change

The assumptions listed in Section 2.5.2 (Gratings) and used to determine diffraction efficiency did not account for material damage or compaction. Compaction effects can be

modeled, but were not include here because they were not measurable within the bulk of a material. Compaction is also accompanied by expansion [34]. The net material expansion and compaction will increase the diffraction efficiency of the gratings. Damages include cracks and voids in the bulk which can scatter and absorb light, confusing the purely phase-shift effect of a pure. It is a source of error in the determination of index modulation from diffraction efficiency. Other errors include differences between theory (rectangular) and practice (cylindrical) in refractive index profile and less than ideal values of waveguide diameter.

It was difficult to compare the grating results directly with the single waveguides because they were not written under the same conditions. The laser power of 2 μJ/pulse used to write some of the waveguides was not obtainable during the grating exposures, for which the maximum power was ~ 1 μJ/pulse. The lower laser power of 0.2 μJ/pulse produced gratings too weak to diffract a visible laser beam. However, by comparing similar scan speed and repetition rate, the general trend that becomes apparent is that the index modulation values from the gratings are larger than those from the waveguides, even at lower energies. The index change values from the gratings measurements as shown in Table 4-1, being significantly larger than any result from the single waveguide NA measurements ($> 8x10^{-3}$ vs. $<4x10^{-3}$), indicate that 1 μJ/pulse energies are also too high and induce excessive damage.

The gratings help to identify damage because the diffraction efficiency of damaged waveguide gratings is much higher than theory. The use of gratings to determine index change is simpler than coupling light into waveguides and measuring numerical aperture. However, low index changes are difficult to measure. For example, 3 μm diameter waveguide gratings with 12 μm spacing requires index changes of $\sim 4x10^{-3}$.

5.2 Comparison with Other Research Groups

5.2.1 Comparison with Cornell University

A primary starting point for this thesis was the research of Gaeta's group at Cornell. They [18] also used the technique of calculating index modulation from NA, however, their method of determining the NA of the waveguides was different that used in this thesis. By using laser light with a NA much larger than the NA of the waveguide, interference between light exiting the waveguides and light not coupled into the waveguide produced a pattern of concentric rings. The radius at which the rings disappeared was used to determine the NA of the waveguide. In this thesis, the NA of the incoming laser diode light was matched as closely as possible to the NA of the waveguides, and the full-width at half maximum (FWHM) of the far-field intensity pattern was then used to find NA.

Gaeta and coworkers [18] characterized both fused silica and BK7 waveguides, with conclusions that achievable BK7 index modulations were ~70% larger than fused silica index modulations: $<5\times10^{-3}$ compared to $<3\times10^{-3}$. The processing window was also larger, encompassing a wider range of writing parameters as defined by the area within the dotted lines in Figure 3-3, which is larger than in Figure 3-4. Additionally, the processing window for BK7 begins at lower accumulated fluences (~600 J/cm^2) than for fused silica (~3500 J/cm^2).

The BK7 waveguides written for this thesis appeared smooth and free of damage spots. Dim light was seen scattering out of the sides of the waveguides, but no coupled light was visible exiting from the side of the guides. BK7 has a smaller bandgap than fused silica. This may explain the higher achievable index modulations. It is possible that the ends of the waveguides were more damaged in the BK7 samples written for this thesis, or perhaps were formed in a manner not conducive to coupling in and out.

In fused silica, the index modulations calculated in this thesis are larger by ~30% than those obtained by Gaeta and coworkers [18] for similar exposure conditions. In addition to the difference in NA measurement methods, two experimental parameters may account for this difference in photosensitivity response: repetition rate and focal diameter.

The 10 and 100 kHz repetition rates at which the waveguides of this thesis were written were higher than the 1 kHz value by Gaeta and coworkers. As was described in Section 5.1.1 (Ultrafast Laser-Written Waveguides), the thermal diffusion distance is vastly different between 1 kHz and 100 kHz. At 100 kHz, pulses arriving after the first pulse interact with a heated and possibly melted material ~6 μm in diameter; whereas at 1 kHz, laser-coupled heat has diffused ~60 μm and the material has cooled substantially from highly excited states. The thermal diffusion effect may be similar to that observed in laser micromachining where high repetition rates or *burst machining* [12] produce a heated region for the laser to interact with. This heated region is more fluid than a cooled lattice, and therefore less susceptible to shock-induced cracking [12]. In the same way, high-repetition rates here may produce a heated volume that permits subsequent laser pulses to increase refractive- index modulation without causing damage.

Another difference between the experiments performed in this thesis and by Gaeta's group [18] is the beam waist diameter. For this thesis, the ultrafast laser was focussed to a diameter of ~3 μm, while Gaeta and coworkers focussed to ~5 μm. This difference provides a ~3-fold increase in intensity at the center of the waveguides and may be responsible for a larger refractive-index change, although not necessarily over the same area cross-section. Focussing to a smaller spot size of ~1 μm, Mazur's group formed storage *bits* through a catastrophic event they termed microexplosions. In modeling the diffraction pattern of a grid of index modulations, their group calculated extremely large

"index modulations" of $50x10^{-3}$ [38]. However, their calculation does not account for the possibility of light scattering and absorption effects that damaged material may present. While Mazur and coworkers found an energy threshold of 0.3 μJ, Hirao and coworkers used a ~4-μm focal diameter and stated a substantially higher threshold energy of 24 mJ [23]. While their definition of threshold levels may be different, the orders of magnitude variation in required energy suggests a focal size dependence which favours stronger interactions with tighter focus.

5.2.2 Comparison with Other Ultrafast Work

The field of ultrafast laser-induced photosensitivity for the writing of optical devices inside glass is relatively new. Within the past two years, the body of literature in this field has been growing rapidly. Pioneering papers [14, 17, 20] often describe new structures and their possible applications.

This thesis focuses largely on mapping a processing range that can be used to enhance the information that has thus far been accumulated. Such information includes the results of Hirao's group [42] summarized in Table 2-1. That group focussed on exploring the variation of pulse energy, pulse width, and number of scans on the propagated modes of the waveguides. This thesis investigated the effects of repetition rate and scan speed on the index modulation, as well as the quality of the waveguides. The new information from this thesis will complement previous work and provide future researchers with guidelines for the fabrication of photonic structures.

The data collected for this thesis was limited by the reliability and available of an ultrafast laser system in our collaborators' laboratory, 450-km outside of Toronto. The laser system broke down during the summer of 2000, precluding a continuation of experiments. Further, many of the waveguide scans produced for this thesis did not result in good

quality waveguides, yielding a scarcity of data. This was further compounded by a narrow processing window with respect to the range of available laser parameters. The results that have been studied support future work that looks to optimize the writing process.

As mentioned previously, much of the research now is focused on novel applications. The work in this thesis builds towards a larger project of this lab: the writing of diffractive 3D photonics. The end goal of this larger project is a free-space device composed of bit and countered modulations, similar to the 3D memory currently being explored. Both this thesis and the phase mask modeling theory used in this thesis [45], work towards this objective. Detailed control over refractive index modulations is required for the construction of designed bit patterns.

5.3 Comparison with UV

As was mentioned in the introduction, index modification of glasses in industry is currently achieved with UV lasers. In this lab, work has been conducted with the 157-nm F_2 laser, which offers the benefit of a photon energy (7.9 eV) close to the bandgap of fused silica (~10 eV). [47].

Figure 5-2 plots index changes over accumulated fluence. Over the same range of accumulated fluence (1,000 to 100,000 J/cm^2), different materials (fused silica and Ge-doped glass) and different lasers (UV and ultrafast) elicit different responses. Index modifications of $1x10^{-4}$ to $3x10^{-4}$ have been achieved by UV lasers in pure fused silica, while in Ge-doped fused silica they reach up to $5x10^{-3}$. Glass with 5% Ge concentration has a bandgap of 7.1 eV, making it a much better absorber of F_2 photons.

Also plotted on the graph are results of ultrafast exposure to pure fused silica (circles). Index changes are also high ($<5x10^{-3}$), however the scatter of the data is larger. This is

due to a measurement method (NA) which is dependent on physical aspects of the waveguide, such as smoothness, that are not fully controllable as yet. In comparison to F_2-laser processing of glasses, ultrafast laser processing is still crude and undeveloped. On the other hand, it offers the advantage of higher index changes (in the same material) and 3D localization.

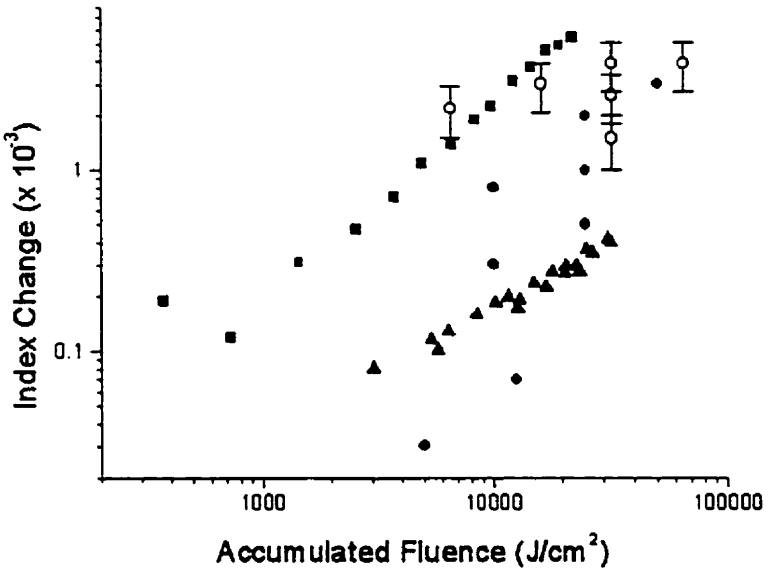

Figure 5-2 Comparison of UV and ultrafast-induced index modifications. ▲ are results of 157 nm on fused silica (Zhang and coworkers [47]). ■ are results of 157 nm on germanium doped fused silica (Chen and coworkers [47]) . ● are results of ultrafast on fused silica (Gaeta and coworkers[18]). ○ are results of ultrafast on fused silica taken for this thesis. Error bars are measurement errors from the calculation of numerical aperture.

5.4 Significance

This thesis has expanded the detailed mapping of a processing window for ultrafast laser-writing of waveguides in fused silica. It has explored the effects of repetition rate and scan speed, suggesting that a thermal effect plays an important role in the induced index modifications and quality of waveguides.

As well, comparisons were made with gratings (diffraction efficiency) to further explore the accuracy of the waveguide index change measurement method (NA). While both schemes are imperfect, an assessment of both together provided insight into their respective flaws.

A comparison with F_2 photosensitivity verifies the index modulation results and illustrates advantages (higher index change, volume localization) as well as disadvantages (lack of control). The lack of control over the process is substantiated by the assessment of the quality of waveguides, which was also conducted in this thesis. This evaluation is important at this stage in directing future research, as well as in providing quantitative reviews for those who wish to employ the waveguides immediately.

Chapter 6

6 CONCLUSIONS

6.1 Summary

The goals of this thesis were to build the knowledge bases that currently exist concerning the magnitude of refractive-index modulations and quality of waveguides written by ultrafast lasers. As for mapping the parameter range to control index change, this thesis has begun to examine the role of such parameters as laser repetition rate and pulse energy. The relationship between Δn and accumulated fluence is not as simple as with UV lasers. General conclusions of this thesis are that a higher repetition rate and tighter focus have the potential to induce higher index changes, although they also increase the likelihood of causing damage. General conclusions of this thesis are that a higher repetition rate and tighter focus have the potential to induce higher index changes, although they also increase the likelihood of causing damage. The processing window for fused silica is quite small: at 10 and 100 kHz, the upper limit is a fluence of ~13 $\mu J/cm^2$, and the number of pulses $<10^5$. The lower limits, as yet identified, are more restricted by processing time to reach a measurable index change. At the same fluence and accumulated fluence, Gaeta observed a maximum Δn of ~$1x10^{-3}$ at 1 kHz, while the results of this thesis demonstrate Δn ~ $2.5x10^{-3}$ at 10 kHz and Δn ~$4x10^{-3}$ at 100 kHz. These values illustrate a significant conclusion of this thesis: the thermal effects associated with faster repetition rates permits higher index changes. This is similar to the

burst machining effect observed in micromachining where fast repetition rates allow laser pulses to keep a sample heated and thus make it more ductile for subsequent pulses.

A waveguide coupling system was designed and constructed to couple light into the bulk waveguides and measure scattering loss and output light. The characterization of the waveguides suggest that slower scan speeds (<50 μm/s) make less lossy waveguides. From a commercial viewpoint, this would be a deterring factor for the use of ultrafast lasers to mass produce large, complicated circuits since the amount of time involved would be too large. Smaller applications such as trimming of circuits and prototyping, however, could still benefit from the flexibility and tunability of ultrafast laser-written waveguides and index bit modulations.

Volume gratings were written in the bulk of fused silica and characterized with measurements of diffraction efficiency to evaluate a different method of calculating index change. Results from the volume gratings helped to narrow the processing window at the upper fluence boundary. However, the method proved ineffectual at lower index change values because of low diffraction efficiencies coupled with practical constraints, such as writing time.

6.2 Future Work

The continuation of this project requires the improvement of laser writing and characterizing procedures used in this thesis. Once this has been accomplished, several new directions can be explored.

A limitation to the quantity and quality of data available for this thesis was the difficulty in measuring light exiting many of the waveguides. Attempts were made to ensure that the ends of the waveguides were not overexposed, however the issue has not been resolved

satisfactorily. Better control over the experimental components is necessary, such as position feedback from the stepper motors.

There are two alternatives to improving the ends of the waveguides that will entail more involved procedures. However, they will provide the opportunity for the benefits of butt coupling, which would increase coupling ease and efficiency. One such option is to write waveguides to the surface of the samples. This is not currently done because of probable ablation at the sample surface. Several schemes that could prevent this are:

- Writing at lower than ablation fluences;
- Using an index matching fluid/gel between the lens and the sample;
- Spinning a polymer onto the surfaces of the sample that can be later removed.

Another alternative to solving the end problem in the waveguides is to remove the excess glass between the ends of the waveguides and the surfaces of the samples. Cleaving is not an option because the glass is amorphous and quite large in size, and the thickness of material to be removed is only several hundred microns. Feasible options are:

- Polishing the surfaces;
- Ablating the surfaces with an F_2 laser.

Once high-quality waveguides can be written reliably, a more detailed exploration of the range of processing parameters can begin. One important parameter is energy per pulse, which should be lowered when attempting to write to the surface. As well, the number of scans and the focussing lens (beam waist diameter) can be varied. The results of this thesis direct future work towards lower energies (~0.2 μJ/pulse) and higher repetition rates (~100 kHz) for writing

pure index modulations without damage. Also, slow scan speeds (<10 μm/s) result in less lossy waveguides.

In terms of characterization, additional experiments include measuring transmission power with a more stable laser source and scattering losses with a more sensitive monochromatic CCD. The transmission spectrum with a white light source on the input and fiber coupler to spectrum analyzer on the output side can be measured. This arrangement of equipment would lead well into the characterization of more characteristics of the waveguides. One such example is birefringence, which can be measured by coupling polarized light into the waveguides. It will be necessary to write longer waveguides for gratings, but a parabolic mirror is now in place in the ultrafast laser system to extend the working distance. Finally, a project at NRC is currently investigating the writing of transverse waveguides (writing perpendicular to the laser beam axis), which may be characterized here in this lab.

As mentioned previously, the ultimate goal of this lab is to write 3D diffractive photonic components. Once confidence has been gained about the effect of all parameters on index modulation, patterns of bits can be written on one plane and then multiple planes, in conjunction with 3D diffractive theory on radiative propagation through index modulations.

REFERENCES

[1] P. Fay, "Exploding market in 1999 creates worldwide fiber shortage," in *Lightwave*, vol. July, 2000, pp. 53-54.

[2] G. P. Agrawal, *Fiber-optic communication systems*, 2nd ed., New York: Wiley, 1997.

[3] M. Lapczyna and M. Stuke, "Rapid prototype fabrication of smooth microreactor channel systems in PMMA by VUV laser ablation at 157 nm for applications in genome analysis and biotechnology," Proceedings of MRS Symposium, San Francisco, CA, USA, 1998.

[4] Y. P. Li and C. H. Henry, "Silica-based optical integrated circuits," *IEE Proceedings Optoelectronics*, vol. 143, pp. 263-80, 1996.

[5] M. Kawachi, "Recent progress in silica-based planar lightwave circuits on silicon," *IEE Proceedings Optoelectronics*, vol. 143, pp. 257-62, 1996.

[6] P. Coudray, P. Etienne, J. Porque, Y. Moreau, and S. I. Najafi, "Integrated optical devices achieved by sol-gel process," *Proceedings of the SPIE The International Society for Optical Engineering*, vol. 3278, pp. 252-8, 1998.

[7] E. M. Yeatman, M. M. Ahmad, O. McCarthy, A. Vannucci, P. Gastaldo, D. Barbier, D. Mongardien, and C. Moronvalle, "Optical gain in Er-doped SiO/sub 2/-TiO/sub 2/ waveguides fabricated by the sol-gel technique," *Optics Communications*, vol. 164, pp. 19-25, 1999.

[8] A. Opilski, R. Rogozinski, K. Gut, M. Blahut, and Z. Opilski, "Present state and perspectives involving application of ion exchange in glass," *Opto Electronics Review*, vol. 8, pp. 117-28, 2000.

[9] P. R. Herman, K. Beckley, and S. Ness, "157-nm photosensitivity in germanosilicate waveguides," Proceedings of Bragg Gratings, Photosensitivity, and Poling in Glass Fibers and Waveguides: Applications and Fundaments, Williamsburg, VA, USA, 1997.

[10] P. Herman, K. Beckley, and S. Ness, "157-nm photosensitivity in germanosilicate and fused-silica glasses," Proceedings of Conference on Lasers and Electro-Optics Conference Edition, San Francisco, CA, USA, 1998.

[11] S. Ness and P. R. Herman, "157-nm photosensitivity in germanosilicate planar waveguides," Proceedings of Conference on Lasers and Electro-Optics, Baltimore, MD, USA, 1999.

[12] P. R. Herman, R. S. Marjoribanks, A. Oettl, K. Chen, I. Konovalov, and S. Ness, "Laser shaping of photonic materials: deep-ultraviolet and ultrafast lasers," *Applied Surface Science*, vol. 154, pp. 577-86, 2000.

[13] K. Miura, Q. Jianrong, T. Mitsuyu, and K. Hirao, "Preparation and optical properties of fluoride glass waveguides induced by laser pulses," *Journal of Non Crystalline Solids*, vol. 256, pp. 212-19, 1999.

[14] Y. Sikorski, A. A. Said, P. Bado, R. Maynard, C. Florea, and K. A. Winick, "Optical waveguide amplifier in Nd-doped glass written with near-IR femtosecond laser pulses," *Electronics Letters*, vol. 36, pp. 226-7, 2000.

[15] K. M. Davis, K. Miura, N. Sugimoto, and K. Hirao, "Writing waveguides in glass with a femtosecond laser," *Optics Letters*, vol. 21, pp. 1729-31, 1996.

[16] E. N. Glezer, M. Milosavljevic, L. Huang, R. J. Finlay, T. H. Her, J. P. Callan, and E. Mazur, "3-D optical storage and engraving inside transparent materials," Proceedings of Topical Meeting Ultrafast Phenomena, San Diego, CA, USA, 1996.

[17] C. Sung Hak, H. Kumagai, K. Midorikawa, and M. Obara, "Fabrication of double cladding structure in optical multimode fibers using plasma channeling excited by a high-intensity femtosecond laser," *Optics Communications*, vol. 168, pp. 287-95, 1999.

[18] D. Homoelle, S. Wielandy, A. L. Gaeta, N. F. Borrelli, and C. Smith, "Infrared photosensitivity in silica glasses exposed to femtosecond laser pulses," *Optics Letters*, vol. 24, pp. 1311-13, 1999.

[19] L. Sudrie, M. Franco, B. Prade, and A. Mysyrowicz, "Writing of permanent birefringent microlayers in bulk fused silica with femtosecond laser pulses," *Optics Communications*, vol. 171, pp. 279-84, 1999.

[20] Y. Kondo, K. Nouchi, T. Mitsuyu, M. Watanabe, P. G. Kazansky, and K. Hirao, "Fabrication of long-period fiber gratings by focused irradiation of infrared femtosecond laser pulses," *Optics Letters*, vol. 24, pp. 646-8, 1999.

[21] K. Hill, Y. Fujii, D. Johnson, and B. Kawasaki, "Photosensitivity in optical fibre waveguides: Application to reflection filter fabrication," *Applied Physics Letters*, vol. 32, pp. 647-9, 1978.

[22] R. Kashyap, *Fiber Bragg Gratings.*, San Diego, CA: Academic Press, 1999.

[23] J. Qiu, K. Miura, H. Inouye, J. Nishii, and K. Hirao, "Three-dimensional optical storage inside a silica glass by using a focused femtosecond pulsed laser," *Nuclear Instruments & Methods in Physics Research, Section B (Beam Interactions with Materials and Atoms)*, vol. 141, pp. 699-703, 1998.

[24] C. Sung Hak, H. Kumagai, K. Midorikawa, and M. Obara, "Double cladding structure in optical multimode fibers fabricated by a high-intensity femtosecond laser," Proceedings of CLEO/Pacific Rim '99. Pacific Rim Conference on Lasers and Electro-Optics, Seoul, South Korea, 1999.

[25] E. N. Glezer, M. Milosavljevic, L. Huang, R. J. Finlay, T. H. Her, T. P. Callan, and E. Mazur, "Three-dimensional optical storage inside transparent materials," *Optics Letters*, vol. 21, pp. 2023-5, 1996.

[26] S. Kawata and A. Toriumi, "Three-dimensional Optical Memory Using Photopolymer, Photorefractive Crystals, and Photochromic Materials," Proceedings of SPIE, 1997.

[27] P. Dietrich, F. Krausz, and P. B. Corkum, "Determining the absolute carrier phase of a few-cycle laser pulse," *Optics Letters*, vol. 25, pp. 16-18, 2000.

[28] P. Mulser, "Theory of Plasma Wave Absorption," in *Laser Interactions with Atoms, Solids, and Plasmas*, R. M. More, Ed. New York, NY: Plenum Press, 1994.

[29] A. S. Dvornikov, I. Cokgor, F. McCormick, R. Piyaket, S. Esener, and P. M. Rentzepis, "Molecular transformation as a means for 3D optical memory devices," *Optics Communications*, vol. 128, pp. 205-10, 1996.

[30] F. Li Chun, H. Si Jin, M. Yang, and X. Wang Yu, "Excited-state nonlinear absorption and its application in photonic technology," *Acta Physica Sinica (Overseas Edition)*, vol. 4, pp. 569-80, 1995.

[31] E. A. Wachter, M. G. Petersen, and H. C. Dees, "Photodynamic therapy with ultrafast lasers," *Proceedings of the SPIE The International Society for Optical Engineering*, vol. 3616, pp. 66-74, 1999.

[32] T. An Chun, S. Backus, H. Kapteyn, M. Murnane, and G. Mourou, "Short-pulse laser damage in transparent materials as a function of pulse duration," *Physical Review Letters*, vol. 82, pp. 3883-6, 1999.

[33] A. Othonos, "Fiber Bragg Gratings," *Review of Scientific Instruments*, vol. 68, pp. 4309-4341, 1997.

[34] K. Hirao and K. Miura, "Writing waveguides and gratings in silica and related materials by a femtosecond laser," *Journal of Non Crystalline Solids*, vol. 239, pp. 91-5, 1998.

[35] K. Miura, Q. Jianrong, H. Inouye, T. Mitsuyu, and K. Hirao, "Photowritten optical waveguides in various glasses with ultrashort pulse laser," *Applied Physics Letters*, vol. 71, pp. 3329-31, 1997.

[36] K. Miura, Q. Jianrong, T. Mitsuyu, and K. Hirao, "Three-dimensional microscopic modifications in glasses by a femtosecond laser," Proceedings of Laser Applications in Microelectronic and Optoelectronic Manufacturing IV, San Jose, CA, USA, 1999.

[37] E. N. Glezer, H. Li, R. J. Finlay, H. Tsing Hau, J. P. Callan, C. Schaffer, and E. Mazur, "Ultrafast laser-induced microexplosions in transparent materials," Proceedings of 28th Annual Boulder Damage Symposium, Boulder, CO, USA, 1997.

[38] E. N. Glezer and E. Mazur, "Ultrafast-laser driven micro-explosions in transparent materials," *Applied Physics Letters*, vol. 71, pp. 882-4, 1997.

[39] C. B. Schaffer, N. Nishimura, and E. Mazur, "Thresholds for femtosecond laser-induced breakdown in bulk transparent solids and water," Proceedings of Time Structure of X-Ray Sources and Its Applications, San Diego, CA, USA, 1998.

[40] C. B. Schaffer, A. Brodeur, N. Nishimura, and E. Mazur, "Microscopic bulk damage in dielectric materials using nanojoule femtosecond laser pulses," Proceedings of Quantum Electronics and Laser Science Conference, Baltimore, MD, USA, 1999.

[41] C. B. Schaffer, A. Brodeur, N. Nishimura, and E. Mazur, "Laser-induced microexplosions in transparent materials: microstructuring with nanojoules," Proceedings of Commercial and Biomedical Applications of Ultrafast Lasers, San Jose, CA, USA, 1999.

[42] K. Hirao and K. Miura, "Writing waveguides in silica-related glasses with femtosecond laser," *Japanese Journal of Applied Physics, Supplement. suppl.*, pp. 49-52, 1998.

[43] Q. Jianrong, K. Miura, and K. Hirao, "Three-dimensional optical memory using glasses as a recording medium through a multi-photon absorption process," *Japanese Journal of Applied Physics, Part 1 (Regular Papers, Short Notes & Review Papers)*, vol. 37, pp. 2263-6, 1998.

[44] C. Sung Hak, H. Kumagai, K. Midorikawa, and M. Obara, "Modification in optical fibers using high-intensity femtosecond lasers," Proceedings of Laser Applications in Microelectronic and Optoelectronic Manufacturing IV, San Jose, CA, USA, 1999.

[45] C. Lauer, "Modeling of phase masks," University of Toronto, Toronto 2000.

[46] A. Y. Naumov, C. Przygodzki, X. Zhu, and P. B. Corkum, "Microstructuring with femtosecond laser inside silica glasses," Proceedings of Conference on Lasers and Electro-Optics, Baltimore, MD, USA, 1999.

[47] P. R. Herman, K. Chen, P. Corkum, A. Naumov, S. Ng, and J. Zhang, "Advanced Laser Microfabrication of Photonic Components," Proceedings of First International Symposium on Laser Precision Microfabrication, Omiya, Saitama, Japan, 2000.